

B meson decay constants from two-flavor lattice QCD with nonrelativistic heavy quarks

A. Ali Khan,¹ S. Aoki,² R. Burkhalter,^{1,2} S. Ejiri,¹ M. Fukugita,³ S. Hashimoto,⁴ N. Ishizuka,^{1,2} Y. Iwasaki,^{1,2} K. Kanaya,^{1,2} T. Kaneko,⁴ Y. Kuramashi,⁴ T. Manke,^{1,*} K. Nagai,¹ M. Okawa,⁴ H. P. Shanahan,^{1,†} A. Ukawa,^{1,2} and T. Yoshiie^{1,2}

(CP-PACS Collaboration)

¹Center for Computational Physics, University of Tsukuba, Tsukuba, Ibaraki 305-8577, Japan

²Institute of Physics, University of Tsukuba, Tsukuba, Ibaraki 305-8571, Japan

³Institute for Cosmic Ray Research, University of Tokyo, Kashiwa, Chiba 277-8582, Japan

⁴High Energy Accelerator Research Organization (KEK), Tsukuba, Ibaraki 305-0801, Japan

(Received 20 March 2001; published 10 August 2001)

We present a study of leptonic B meson decay constants in lattice QCD with two flavors ($N_f=2$) of light dynamical quarks using nonrelativistic QCD for the heavy quark. Gauge configurations are generated with a renormalization-group improved gauge action and a mean-field-improved clover light quark action. Measurements are carried out at two values of $\beta=6/g^2$, each for four sea quark masses, corresponding to inverse lattice spacings $a^{-1}\approx 1.3$ and 1.8 GeV in the chiral limit of the sea quark. The continuum values of the decay constants are derived by evaluating the discretization errors at each finite lattice spacing. We find $f_B^{N_f=2} = 204(8)(29)(+44)$ MeV, $f_{B_s}^{N_f=2} = 242(9)(34)(+38)$ MeV, and $f_{B_s}^{N_f=2}/f_B^{N_f=2} = 1.179(18)(23)$, where the errors listed are statistical, systematic and uncertainty due to choice of the physical quantity used to fix the scale. Comparison is made to quenched results ($N_f=0$) obtained with the same action combination and matching lattice spacings. We find $f_B^{N_f=2}/f_B^{N_f=0} = 1.07(5)$, $f_{B_s}^{N_f=2}/f_{B_s}^{N_f=0} = 1.10(5)$ and $(f_{B_s}/f_B)^{N_f=2}/(f_{B_s}/f_B)^{N_f=0} = 1.03(2)$, which indicate a 5–10 % increase in the values of the decay constants, but no appreciable change in the ratio f_{B_s}/f_B , due to sea quarks.

DOI: 10.1103/PhysRevD.64.054504

PACS number(s): 12.38.Gc

I. INTRODUCTION

An accurate determination of the B meson decay constant has practical importance, as it is needed, together with the $\bar{B}-B$ transition matrix elements, for the extraction of the quark mixing matrix elements from the $\bar{B}-B$ mass difference. To this end much effort has been put toward a quantitative evaluation of these matrix elements using lattice QCD (for reviews, see Refs. [1,2]).

A problem specific to heavy meson calculations with the original lattice formulation is that the heavy quark mass is greater than unity in units of the lattice spacing, which makes the lattice artifacts intolerably large. There are two popular formalisms to handle heavy quarks, using the fact that the heavy quark in a B meson is nonrelativistic, in a way that large discretization effects proportional to the heavy quark mass do not appear. One is the use of a relativistic action with the aid of a nonrelativistic reinterpretation (the Fermilab formalism) [3], and the other is simulations with the nonrelativistic QCD (NRQCD) action [4].

The problem with these formalisms, however, is that a continuum extrapolation is not simple. For instance, since the NRQCD action is not renormalizable, an infinite number of terms is involved in the $aM\rightarrow 0$ limit, and their matching to the continuum theory requires good control of a power

divergence of the form $1/(aM)^n$ with n a positive integer. In the Fermilab formalism the continuum extrapolation is possible in principle, although it is difficult in practice because of the complicated a dependence of the couplings in the effective Hamiltonian of the heavy quark. Therefore, an estimation of systematic errors arising from the continuum extrapolation is a nontrivial task in both formalisms.

Another uncertainty in previous calculations of heavy mesons is the effect of dynamical quarks. Most lattice studies to date adopted the quenched approximation. There are two calculations in which dynamical quarks are incorporated (full QCD) [6,7]. The results indicate that the inclusion of dynamical quarks increases the value of f_B and f_{B_s} . However, study by Collins *et al.* [6], using NRQCD for heavy quarks and the clover action for light valence quarks, was made only at a single lattice spacing in a small physical volume, and with the Kogut-Susskind staggered action for sea quarks with a mass near to that of the strange quark. The other study by the MILC Collaboration [7], while covering a range of lattice spacings and sea quark masses, used the Wilson action both for heavy and light valence quarks, but employed the staggered action for sea quarks. The problem with these calculations are that the actions for valence and sea quarks are different, having different symmetry structures at finite lattice spacings. This would be an additional source of systematic errors.

We study the B meson decay constants f_B and f_{B_s} , incorporating two flavors of light dynamical quarks, which are identified as u and d quarks. The strange quark is treated in the quenched approximation. In order to test the estimation of systematic errors in the final results in the continuum

*Present address: Department of Physics, Columbia University, New York, New York 10027.

†Present address: Department of Biochemistry and Molecular Biology, University College London, London, United Kingdom.

limit, we compare the results from the two heavy quark formalisms. The work with the Fermilab formalism was published separately [5]. In this paper, we present the calculation using NRQCD.

We carry out full QCD calculations with a consistent use of a quark action for both sea and light valence quarks. We adopt a renormalization group improved gauge action [8] for the gluon sector and an $O(a)$ -improved clover action [9] for sea and light valence quarks [10–12]. The use of the improved action enables us to reduce discretization errors, and makes it possible to study decay constants at moderate lattice spacing, which is feasible with the present computer resource.

The full QCD calculation is performed at two lattice spacings ($1/a \approx 1.3$ and 1.8 GeV). In order to study the dynamical quark effects, we perform parallel quenched simulations with the same action, tuning the lattice spacing to be the same as those in full QCD simulations.

The outline of this paper is as follows. In Sec. II, we introduce the lattice formulations of NRQCD used in this calculation, and define the operators that contribute to the axial vector current. Simulation details such as the run parameters and the choice of operators, and fitting methods, are described in Sec. III. In Sec. IV, we discuss determinations of the physical lattice spacing, the B meson masses and decay constants. A detailed discussion of the extrapolation and interpolation to the physical quark masses is given. We then attempt to obtain the continuum results by estimating the discretization errors at each finite lattice spacing in Sec. V. A comparison with results of previous studies is made in Sec. VI, and the conclusions are given in Sec. VII. Detailed numerical results are collected in some of the tables.

II. FORMALISM

A. Actions

For gluons we adopt a renormalization-group (RG) improved gauge action consisting of plaquettes and 1×2 rectangular Wilson loops [8]. The action for both sea quarks and light valence quarks is taken to be the $O(a)$ -improved clover action [9] with a mean-field-improved clover coefficient $c_{SW} = P^{-3/4}$, where the plaquette P is evaluated in one-loop perturbation theory as $P = 1 - 0.8412/\beta$. For our choice of parameters the measured values of plaquette $\langle P \rangle$ is well approximated by the one-loop evaluation [12].

For the heavy quarks we use NRQCD corrected to $O(1/M_0)$ with M_0 the heavy quark mass. Previous quenched NRQCD calculations showed that $O(1/M_0^2)$ corrections are small in the decay constants, being of the order of $\sim 3\text{--}4\%$ at the lattice spacings used in this study [13–15]. There are various ways to discretize a NRQCD action (see e.g., Refs. [4,14,16]). Here, we choose an action that is symmetric under a time reversal transformation,

$$S_{NRQCD} = \sum \psi_t^\dagger \left[\psi_t - \left(1 - \frac{a\delta H}{2} \right)_t \left(1 - \frac{aH_0}{2n} \right)_t^n \right. \\ \left. \times U_4^\dagger \left(1 - \frac{aH_0}{2n} \right)_{t-1}^n \left(1 - \frac{a\delta H}{2} \right)_{t-1} \psi_{t-1} \right], \quad (1)$$

TABLE I. Full QCD run parameters.

$\beta = 1.95$ on a $16^3 \times 32$ lattice				
K_{sea}	0.1375	0.1390	0.1400	0.1410
# config	648	505	670	397
K_{val}	0.1375	0.1375	0.1375	0.1375
	0.1390	0.1390	0.1390	0.1390
	0.1400	0.1400	0.1400	0.1400
	0.1410	0.1410	0.1410	0.1410
	0.1415	0.1415	0.1415	0.1415
(aM_0, n)	(2.4,2)	(2.4,2)	(2.4,2)	(2.4,2)
	(2.9,2)	(2.9,2)	(2.9,2)	(2.9,2)
	(3.4,2)	(3.4,2)	(3.4,2)	(3.4,2)
	(4.0,2)	(4.0,2)	(4.0,2)	(4.0,2)
	(4.8,2)	(4.8,2)	(4.8,2)	(4.8,2)
 $\beta = 2.1$ on a $24^3 \times 48$ lattice				
K_{sea}	0.1357	0.1367	0.1374	0.1382
# config	400	403	379	420
K_{val}	0.1357	0.1357	0.1357	0.1357
	0.1364	0.1364	0.1364	0.1364
	0.1374	0.1374	0.1374	0.1374
	0.1382	0.1382	0.1382	0.1382
	0.1385	0.1385	0.1385	0.1385
 (aM_0, n)				
	(2.4,2)	(2.4,2)	(2.4,2)	(2.4,2)
	(2.6,2)	(2.6,2)	(2.6,2)	(2.6,2)
	(2.9,2)	(2.9,2)	(2.9,2)	(2.9,2)
	(3.2,2)	(3.2,2)	(3.2,2)	(3.2,2)
	(3.5,2)	(3.5,2)	(3.5,2)	(3.5,2)

where ψ_t is a two-component Pauli spinor at a time slice t . The sum runs over all lattice sites, while indices to represent spatial positions are suppressed. The operators H_0 and δH correspond to the nonrelativistic kinetic energy and the spin-chromomagnetic interaction, as defined by

$$H_0 \equiv -\frac{\Delta^{(2)}}{2M_0}, \quad (2)$$

$$\delta H \equiv -c_B \frac{g}{2M_0} \vec{\sigma} \cdot \vec{B}, \quad (3)$$

respectively, where $\Delta^{(2)}$ is a Laplacian discretized in a standard way and \vec{B} represents a chromomagnetic field strength defined with a clover-leaf shape as in Ref. [4]. The stabilization parameter n is introduced to avoid an instability of the Green's function at large separation due to high-momentum modes. In the free theory, this parameter should satisfy $n > 3/(2aM_0)$ [4]. We choose a larger value of n to make the simulation stable [14,15]. The actual numbers are given in Table I for full QCD runs and in Table II for quenched QCD runs. Gauge links appearing in the NRQCD action are mean-field-improved, $U_\mu \rightarrow U_\mu/u_0$, with u_0 determined from the mean link in the Landau gauge. The coefficient c_B is set to its tree-level value, i.e., unity. We allow the heavy quark

TABLE II. Quenched run parameters.

β	2.187	2.281	2.334	2.575
lattice	$16^3 \times 32$	$16^3 \times 32$	$16^3 \times 32$	$24^3 \times 48$
# config	195	200	200	200
K_{val}	0.1351	0.1343	0.1337	0.1329
	0.1365	0.1357	0.1349	0.1337
	0.1375	0.1367	0.1358	0.1344
	0.1385	0.1377	0.1368	0.1351
	0.1390	0.1383	0.1374	0.1353
(aM_0, n)	(2.4,2)	(2.4,2)	(2.4,2)	(2.4,2)
	(2.9,2)	(2.9,2)	(2.9,2)	(2.6,2)
	(3.4,2)	(3.4,2)	(3.4,2)	(2.9,2)
	(4.0,2)	(4.0,2)	(4.0,2)	(3.2,2)
	(4.8,2)	(4.8,2)	(4.8,2)	(3.5,2)

Green's functions to evolve from $t=0$ to $T/2$, and a time reversed evolution through the second half of the lattice from the same source.

B. Current operators

The pseudoscalar decay constant is defined by

$$if_B p_\mu = \langle 0 | A_\mu | B(p) \rangle, \quad (4)$$

where the axial current $A_\mu = \bar{q} \gamma_5 \gamma_\mu h$ is formed with the relativistic spinors q for the light quark and h for the heavy quark. We restrict our considerations to the time component A_0 .

The heavy quark field h is related to a nonrelativistic field Q via a Foldy-Wouthuysen-Tani transformation at tree level. Ignoring the $O(1/M^2)$ terms, this reads

$$h = \left(1 - \frac{\vec{\gamma} \cdot \vec{\nabla}}{2M_0} \right) Q, \quad (5)$$

where

$$Q = \begin{pmatrix} \psi \\ 0 \end{pmatrix}. \quad (6)$$

We write the two lattice operators contributing to the time component of the heavy-light axial vector current as

$$\begin{aligned} J_L^{(0)} &= \bar{q} \gamma_5 \gamma_0 Q, \\ J_L^{(1)} &= -\frac{1}{2M_0} \bar{q} \gamma_5 \gamma_0 \vec{\gamma} \cdot \vec{\nabla} Q. \end{aligned} \quad (7)$$

In matching the continuum operator to the lattice counterparts, an additional operator $J_L^{(2)}$ appears at $O(1/M)$,

$$J_L^{(2)} = \frac{1}{2M_0} \bar{q} \vec{\gamma} \cdot \vec{\nabla} \gamma_5 \gamma_0 Q, \quad (8)$$

though its matrix element is equal to that of $J_L^{(1)}$ at zero momentum due to translational invariance on the lattice. Thus at the one-loop level we use

$$A_0 = (1 + \alpha_s \rho_A^{(0)}) J_L^{(0)} + (1 + \alpha_s \rho_A^{(1)}) J_L^{(1)} + \alpha_s \rho_A^{(2)} J_L^{(2)}, \quad (9)$$

where $\rho_A^{(0)}$, $\rho_A^{(1)}$ and $\rho_A^{(2)}$ were computed in Ref. [17]¹ for the RG-improved gauge action. The coefficient $\rho_A^{(2)}$ diverges in the limit of $aM_0 \rightarrow \infty$ as $0.34 \times 2aM_0$, which cancels the factor $1/M_0$ in the definition of $J_L^{(2)}$ and gives a finite contribution. This remaining contribution corresponds to the improvement of discretization error of $O(\alpha_s a)$ [18] in the static limit.

For α_s , we use the coupling defined with the modified minimal subtraction ($\overline{\text{MS}}$) scheme at $\mu = 1/a$, which is evaluated using the one-loop relation

$$\begin{aligned} \frac{1}{g_{\overline{\text{MS}}}^2(\mu)} &= \frac{(c_0 P - 8c_1 R)\beta}{6} - 0.1006 + \frac{22}{16\pi^2} \log(\mu a) \\ &+ N_f \left(0.03149 - \frac{4}{48\pi^2} \log(\mu a) \right). \end{aligned} \quad (10)$$

The mean-field improvement is applied using measured values of the 1×1 and 1×2 Wilson loops P and R .

III. SIMULATION DETAILS

A. Gauge configurations

The CP-PACS Collaboration generated a set of full QCD gauge configurations incorporating two flavors of light dynamical quarks at four values of gauge coupling, $\beta = 1.8$, 1.95, 2.1, and 2.2, using the hybrid Monte Carlo (HMC) algorithm [10–12]. At each β , four sea quark masses m_{sea} are chosen in the range $0.5m_s \leq m_{sea} \leq 3m_s$, where m_s denotes the strange quark mass. In the chiral limit of sea quarks, these couplings correspond to lattice spacings a with $1 \text{ GeV} \lesssim a^{-1} \lesssim 2.2 \text{ GeV}$. The spatial lattice size is about 2.5 fm at $\beta = 1.8$, 1.95, and 2.1, while it is about 1.9 fm at $\beta = 2.2$. The parameters of the configurations are summarized in the left half of Table III.

In the present study we use the configurations at $\beta = 1.95$ ($a^{-1} \approx 1.3 \text{ GeV}$) and 2.1 ($a^{-1} \approx 1.8 \text{ GeV}$); all the gauge configurations we generated are analyzed at $\beta = 1.95$, whereas half the configurations, corresponding to the first 2000 trajectories, are employed for $\beta = 2.1$. The configurations are separated by ten HMC trajectories at $\beta = 1.95$ and by five trajectories at 2.1. We discard configurations at $\beta = 1.8$, because of expected large discretization errors, and at $\beta = 2.2$ for too small a physical volume. Details of the parameters employed in our analysis are listed in Table III.

¹The definition of the lattice currents $J_4^{(i)}$ in Ref. [17] is slightly different from that of $J_L^{(i)}$ used in this paper. The tree level rotation is included in $J_4^{(0)}$ in Ref. [17]. The one-loop coefficients $\rho_A^{(i)}$ are modified accordingly.

TABLE III. Overview of full QCD and quenched configurations. The scale a_σ , fixed by assuming $\sqrt{\sigma} = 440$ MeV, is shown to illustrate the matching of scales (measurement of σ at $\beta=2.10$ is made for the first 2000 trajectories). The quenched runs have 200 configurations for each β .

Full QCD simulations						Quenched simulations			
lattice	β	c_{SW}	K_{sea}	# traj.	m_π/m_ρ	a_σ (fm)	β	c_{SW}	a_σ (fm)
$12^3 \times 24$	1.80	1.60	0.1409	6250	0.806(1)	0.289(3)			
			0.1430	5000	0.753(1)	0.280(4)			
			0.1445	7000	0.696(2)	0.269(3)			
			0.1464	5250	0.548(4)	0.248(2)			
$16^3 \times 32$	1.95	1.53	0.1375	7000	0.805(1)	0.204(1)	2.187	1.439	0.2079(15)
			0.1390	7000	0.751(1)	0.193(2)	2.214	1.431	0.1977(13)
			0.1400	7000	0.688(1)	0.181(1)	2.247	1.422	0.1853(9)
			0.1410	7000	0.586(3)	0.170(1)	2.281	1.412	0.1727(10)
$24^3 \times 48$	2.10	1.47	0.1357	4000	0.806(1)	0.1342(6)	2.416	1.379	0.1359(7)
			0.1367	4000	0.755(2)	0.1259(5)	2.456	1.370	0.1266(13)
			0.1374	4000	0.691(3)	0.1201(5)	2.487	1.363	0.1206(9)
			0.1382	4000	0.576(3)	0.1128(3)	2.528	1.355	0.1130(9)
$24^3 1 \times 48$	2.20	1.44	0.1351	2000	0.800(2)	0.1049(2)			2.575
			0.1358	2000	0.752(3)	0.1012(3)			
			0.1363	2000	0.702(3)	0.0977(3)			
			0.1368	2000	0.637(6)	0.0947(2)			

The CP-PACS study of full QCD is supplemented by quenched simulations. These simulations are based on a set of quenched configurations with the same gauge action separated by 100 sweeps, each sweep consisting of one heatbath step and four overrelaxation steps. The gauge couplings in the quenched configurations are tuned such that the string tension matches the one in full QCD at four sea quark masses in our simulation and at the physical sea quark mass point corresponding to u and d quarks, as shown in the right half of Table III [5]. We analyze a subset of the quenched configurations at four values of β as listed in Table II. The first two values ($\beta=2.187$ and 2.281) correspond to full QCD runs with the heaviest and the lightest sea quark masses at $\beta=1.95$. The third ($\beta=2.334$) and fourth ($\beta=2.575$) values correspond to full QCD at $\beta=1.95$ and 2.1 at the physical sea quark mass, respectively. Details of the parameters of these quenched runs are given in Table II.

B. Correlator measurements

In order to improve the overlap of interpolating field with the heavy-light meson ground state, we use smeared operators O_S ,

$$O_S(\vec{x}, t) = \sum_{\vec{y}} \bar{q}(\vec{x}, t) \gamma_5 Q(\vec{y}, t) \phi(|\vec{x} - \vec{y}|), \quad (11)$$

on the gauge configurations fixed to the Coulomb gauge. For the smearing function $\phi(|\vec{x} - \vec{y}|)$ we use an exponential form

$$\phi(|\vec{x} - \vec{y}|) = A \exp(-B|\vec{x} - \vec{y}|) \quad \text{for } |\vec{x} - \vec{y}| \neq 0, \quad (12)$$

$$\phi(0) = 1.$$

We calculate correlators using smeared operators at the source and using both local and smeared operators at the sink,

$$C_{SS}(t) = \sum_{\vec{x}} \langle O_S(\vec{x}, t) O_S^\dagger(\vec{0}, 0) \rangle, \quad (13)$$

$$C_{SL}(t, |\vec{p}|) = \sum_{\vec{x}} e^{i\vec{p} \cdot \vec{x}} \langle O_L(\vec{x}, t) O_S^\dagger(\vec{0}, 0) \rangle,$$

where O_L denotes a local pseudoscalar density. The spatial momentum \vec{p} is introduced for C_{SL} to study the energy-momentum dispersion relation of mesons. We make measurements for momenta $p^2 = |\vec{p}|^2 = 0, 1, \dots, 5$ in units of $(2\pi/La)^2$ with L the spatial extent of the lattice. We average over all possible spatial directions.

The correlators for the axial currents are given by

$$C_{SL}^{(i)}(t) = \sum_{\vec{x}} \langle J_L^{(i)}(\vec{x}, t) O_S^\dagger(\vec{0}, 0) \rangle, \quad i=0, 1, 2. \quad (14)$$

Note that $C_{SL}^{(0)}(t) \equiv C_{SL}(t, \vec{0})$ since the lower two components of Q vanish.

C. Correlator fits

To calculate the decay constants we need the amplitude of the local currents. Since smeared-smeared and smeared-local

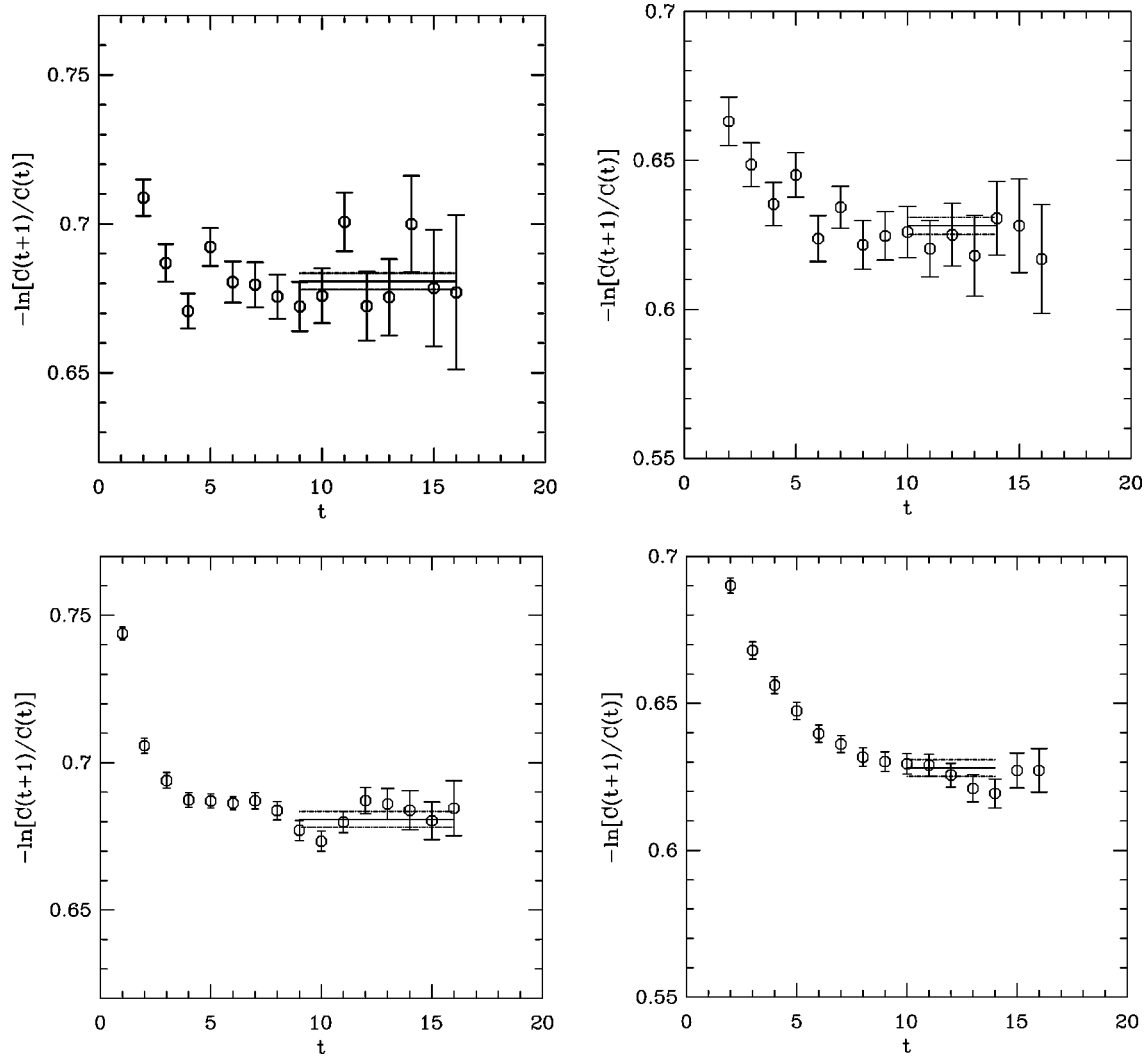


FIG. 1. Upper panels show the effective mass of C_{SS} (left) and $C_{SL}^{(0)}$ (right) in full QCD at $\beta=1.95$, $K_{sea}=0.1410$, $K_{val}=0.1390$, and $aM_0=4.0$. Lower panels are for quenched QCD at $\beta=2.334$ for $K=0.1349$ and $aM_0=4.0$. Solid and dashed lines show fit results and one standard deviation error band.

correlators both have an exponential falloff with the same exponent controlled by E_{sim} , we make a simultaneous fit to a single exponential as

$$C_{SS}(t)=Z_S^2 \exp(-E_{sim}t), \quad (15)$$

$$C_{SL}^{(i)}(t)=Z_L^{(i)}Z_S \exp(-E_{sim}t), \quad i=0,1,2. \quad (16)$$

We apply a bootstrap procedure with 500 samples, taking correlations between different correlators and time slices into account. For the dynamical configurations, we bin over two configurations at $\beta=1.95$ and five configurations at $\beta=2.1$. The quenched configurations are regarded as independent and are not binned. Results from forward and time reversed evolution on the same configurations are always averaged. In the full QCD analysis at $\beta=2.1$ we introduce a cutoff on the ratio of the largest to the smallest eigenvalues of the covariance matrix to avoid a low value of the goodness of fit Q . For the heaviest and lightest sea quark masses we checked

that the effect of this procedure on the decay constants is small, amounting to at most $\sim 25\%$ of the statistical error. The problem of a low Q at $\beta=2.1$ might arise from the smaller number of independent configurations.

The fitting interval $[t_{min}, t_{max}]$ is chosen such that both correlators already reach a plateau at t_{min} . This is judged by Q , as well as by eye from the effective mass and effective amplitude plots. Correlators, in particular C_{SS} , are often dominated by noise for large t , which is indicated by a decrease of Q for a large t_{max} . We cut the fit at t_{max} before noise dominates.

Examples of the effective mass plots for $C_{SL}^{(0)}$ and C_{SS} are shown in Figs. 1 and 2, where the light valence quark mass is taken approximately to be the strange quark mass and the heavy quark mass to be the b quark. In Fig. 1 the upper two panels illustrate full QCD data at $\beta=1.95$ with the lightest sea quark mass, and the lower two show quenched results at $\beta=2.334$ corresponding to the physical value of the sea quark mass in full QCD at $\beta=1.95$. Figure 2 shows similar plots at $\beta=2.1$.

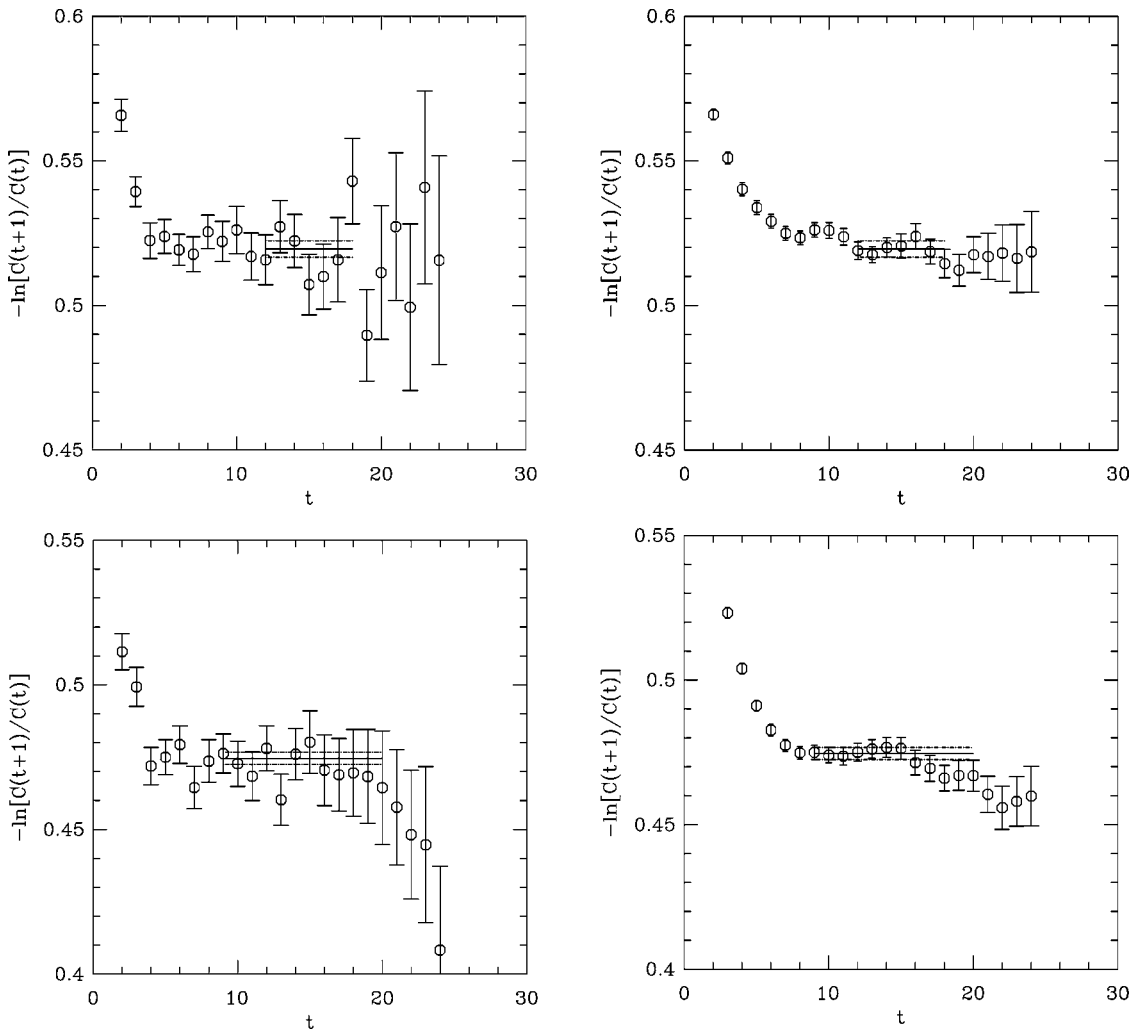


FIG. 2. Upper panels show the effective mass of C_{SS} (left) and $C_{SL}^{(0)}$ (right) in full QCD at $\beta=2.1$, $K_{sea}=0.1382$, $K_{val}=0.1374$, and $aM_0=2.9$. Lower panels are for quenched QCD at $\beta=2.575$, $K_{val}=0.1374$, and $aM_0=2.9$.

Energy for a given finite spatial momentum $E_{sim}(p^2)$ is extracted from the difference $\Delta E(p^2) \equiv E_{sim}(p^2) - E_{sim}(0)$ using a single exponential fit to the ratio

$$\frac{C_{SL}(t, |\vec{p}|)}{C_{SL}(t, |\vec{0}|)} = A(|\vec{p}|) \exp[-\Delta E(p^2)t]. \quad (17)$$

An example of the effective mass is shown in Fig. 3 for full QCD simulations at $\beta=2.1$.

IV. ANALYSIS

A. Fixing the physical scale

We carry out a partially quenched analysis of the dynamical configurations. That is, we evaluate the decay constants for the configurations at each sea quark mass, at which the lattice spacing and physical quark masses are determined by varying the valence light quark mass as we do in the quenched analysis. We then extrapolate the results to the physical value of the sea quark mass. In this subsection we discuss the determination of the lattice scale.

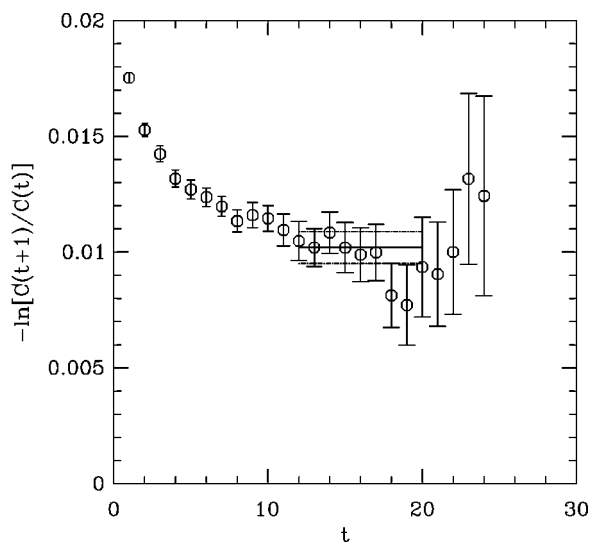


FIG. 3. Effective mass plot of the ratio of correlators at $p=2\pi/L$ and at $p=0$ for $\beta=2.1$, and $K_{sea}=0.1382$. Valence quark masses correspond to $K_{val}=0.1374$ and $aM_0=2.9$.

TABLE IV. Lattice spacings and physical values of the valence hopping parameter K for full QCD.

β	1.95				
K_{sea}	0.1375	0.1390	0.1400	0.1410	physical
$\alpha_{\overline{MS}}(1/a)$	0.2241	0.2241	0.2241	0.2241	0.2241
K_c	0.144221(10)	0.143648(11)	0.143214(13)	0.142737(11)	0.142065(13)
a_ρ^{-1} (GeV)	0.990(4)	1.048(5)	1.097(6)	1.191(9)	1.269(14)
K_l	0.144056(10)	0.143498(11)	0.143073(13)	0.142613(11)	0.141998(12)
$K_s(K)$	0.13998(4)	0.13979(4)	0.13960(4)	0.13956(5)	0.13928(6)
$K_s(\Phi)$	0.13908(6)	0.13896(7)	0.13885(7)	0.13899(8)	0.13863(8)
a_Y^{-1} (GeV)	1.115(8)	1.185(25)	1.242(12)	1.337(15)	1.469(53)
K_l	0.144091(10)	0.143530(11)	0.143104(12)	0.142638(10)	
$K_s(K)$	0.140870(8)	0.140608(9)	0.140373(8)	0.140190(10)	
$K_s(\Phi)$	0.13965(4)	0.13949(4)	0.13935(4)	0.13940(5)	
β	2.1				
K_{sea}	0.1357	0.1367	0.1374	0.1382	physical
$\alpha_{\overline{MS}}(1/a)$	0.204	0.204	0.204	0.204	0.204
K_c	0.139748(19)	0.13954(3)	0.139388(13)	0.139238(10)	0.139022(19)
a_ρ^{-1} (GeV)	1.435(15)	1.529(12)	1.579(16)	1.670(24)	1.789(35)
K_l	0.139652(19)	0.13945(3)	0.139306(11)	0.139160(10)	0.138967(18)
$K_s(K)$	0.13730(5)	0.13732(4)	0.13727(4)	0.13727(6)	0.13726(7)
$K_s(\Phi)$	0.13686(10)	0.13701(8)	0.13700(7)	0.13701(10)	0.13701(10)
a_Y^{-1} (GeV)	1.772(25)			2.010(35)	
K_l	0.139684(18)			0.139183(9)	
$K_s(K)$	0.138111(10)			0.137835(9)	
$K_s(\Phi)$	0.13740(6)			0.13737(5)	

In simulations of full QCD with the realistic spectrum of dynamical sea quarks, one should in principle obtain a unique value for the lattice spacing a from any physical quantity. In our simulation, however, we obtain different values of a depending on the quantity used to fix the scale since dynamical quark effects other than those of u and d quarks are not included.

One way to determine the lattice spacings is to use the ρ meson mass. We refer the reader to Refs. [10–12] for the light hadron spectroscopy calculation, from which we constructed Tables IV and V.

Another way is to use Y level splittings. Specifically, we take the spin-averaged $1P - 1S$ splitting, which is considered

to be relatively insensitive to systematic errors. Our study of the Y spectroscopy using the NRQCD action was described in Ref. [19].

One may think that the most natural scale for the physics of B mesons is their level splittings. In quenched studies [20,21], it was found that the scale from the spin-independent B spectrum agrees with that from the ρ meson mass. We defer a verification in full QCD to a separate work. In this study, we study the scale from the ρ meson mass, denoted as a_ρ in the following, and that from the $Y 1P - 1S$ splitting, denoted as a_Y . We do not adopt the string tension to fix the scale, because its physical value is not well known.

TABLE V. Lattice spacings and physical values of the hopping parameter K for the quenched QCD runs.

β	2.187	2.281	2.334	2.575
$\alpha_{\overline{MS}}(1/a)$	0.2242	0.2122	0.2062	0.1829
K_c	0.141666(12)	0.139587(15)	0.138728(13)	0.136116(8)
a_ρ^{-1} (GeV)	1.017(10)	1.116(12)	1.207(12)	1.743(17)
K_l	0.141504(12)	0.139451(14)	0.138604(13)	0.136036(7)
$K_s(K)$	0.13747(8)	0.13609(8)	0.13552(6)	0.13409(4)
$K_s(\Phi)$	0.13651(15)	0.13522(15)	0.13477(11)	0.13368(7)
a_Y^{-1} (GeV)	1.197(19)	1.397(16)		
K_l	0.141557	0.139510		
$K_s(K)$	0.138824	0.137351		
$K_s(\Phi)$	0.137421	0.136161		

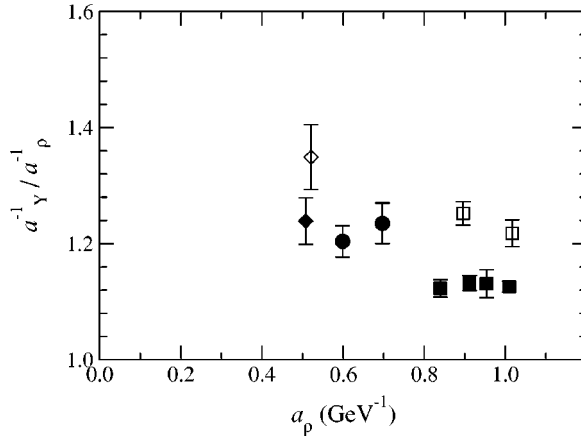


FIG. 4. Ratio of inverse lattice spacings from $\Upsilon(1P - 1S)$ and m_ρ for full (filled symbols) and quenched (open symbols) QCD. Our results for $N_f=2$ (partially quenched) lattices are denoted by filled squares ($\beta=1.95$) and filled circles ($\beta=2.1$) [19]. The open and filled diamonds denote a quenched [14,23] and partially quenched [6] result, respectively, for the plaquette gauge action. Error bars are purely statistical.

Our results for the lattice spacings are listed in Tables IV and V for unquenched and quenched lattices respectively. Note that a_ρ given in this paper differs slightly from the one presented in Ref. [19], the latter being calculated in the chiral limit where the (u,d) quark mass vanishes rather than at the physical point. The ratio of the scales is plotted in Fig. 4 for quenched (open symbols) and full (filled symbols) QCD. The ratio becomes closer to unity with the inclusion of a dynamical quark, but the discrepancy still remains significant. We note that the discrepancy does not decrease toward the continuum limit.

The light quark mass corresponding to the u and d quarks is determined from m_π . To determine the strange quark mass, we use either the K meson mass or the ϕ meson mass. The corresponding hopping parameters, denoted by K_l , $K_s(K)$ and $K_s(\phi)$, are given in Tables IV and V.

B. B meson masses

In NRQCD, the exponential falloff of the correlator in Euclidean time, E_{sim} , represents the bare binding energy. We expect that the nonperturbative mass of heavy-light mesons is inferred from the meson dispersion relation. We use the relativistic form

$$\Delta E(p^2) \equiv E_{sim}(p^2) - E_{sim}(0) = \sqrt{M_{kin}^2 + p^2} - M_{kin}. \quad (18)$$

In practice, we determine this energy difference from a fit of the ratio of the correlators at $p^2=(2\pi/La)^2$ and $p^2=0$ to a single exponential. The results are given in Table VI for full QCD and in Table VII for the quenched case. We also examine this particular form of the dispersion relation by comparing the results using momenta larger than one lattice unit, and find that they agree within errors. An example for M_{kin} as a function of p^2 is given in Fig. 5 for a quenched lattice at $\beta=2.575$.

The meson masses can also be estimated from E_{sim} , through the perturbative relation

$$M_{pert} = E_{sim} + \Delta_{pert} \equiv E_{sim} + Z_m M_0 - E_0, \quad (19)$$

where Z_m is the quark mass renormalization constant, and E_0 is a shift of the zero point of the energy that occurs in non-relativistic and static theories. We employ one-loop perturbative values of Z_m and E_0 [17], using $\alpha_{\overline{\text{MS}}}$ as defined in Eq. (10) at the scale $1/a$. Results for E_{sim} are given in Tables VIII and IX, and those for M_{pert} in Tables X and XI.

The statistical errors in E_{sim} are very small. The error of M_{pert} quoted in these tables is dominated by the systematic error from higher order radiative corrections, as estimated by $\alpha_{\overline{\text{MS}}}^2(1/a)$ times the meson mass. We find that the one-loop contribution to Δ_{pert} is always smaller than our estimate of the two-loop error, which increases our confidence in the error estimate.

For light valence quark masses around m_s , M_{kin} , and M_{pert} agree within the combined errors for all configurations except for those for $\beta=2.1$, for $K_{sea}=0.1357$ in full QCD, and for $\beta=2.575$ in quenched QCD. Even for these cases the difference is at most two standard deviations of the statistical error in M_{kin} . In Fig. 6 we show a comparison between M_{kin} and M_{pert} for full (top panel) and quenched QCD (bottom panel) at our finest lattice spacing of $a_\rho^{-1} \approx 1.8 \text{ GeV}$. The full QCD data show an agreement which is typical of our data, while for the quenched data we show the case of the largest discrepancy.

To determine the bare b quark mass M_{0b} , we employ the kinetic meson mass M_{kin} , as it is free from higher order perturbative errors. The systematic uncertainty in the choice of the method will be discussed later. We first fit the mass as a linear function of the light quark mass,

$$M = A_q + \frac{B_q}{2} \left(\frac{1}{K} - \frac{1}{K_c} \right), \quad (20)$$

and extrapolate or interpolate to the physical value K_l and K_s to obtain the heavy-light meson masses M_l and M_s . The result is then expressed as a function of the heavy quark mass, as

$$M_{l,s} = A_Q M_0 + B_Q, \quad (21)$$

and M_{0b} is determined by requiring M_l or M_s to equal the physical meson mass, M_B or M_{B_s} , respectively.

Examples for these fits in the light and heavy quark mass are given in Fig. 7. On the right panel, a plot of M_s/M_0 is shown as a function of $1/M_0$, which is $A_Q + B_Q/M_0$. Results using the B meson agree with those from B_s allowing for larger errors. We use the B_s meson rather than the B meson to calculate the central values of M_{0b} to avoid the larger statistical and possible systematic errors from the extrapolation to K_l . The difference between the use of the K and ϕ mesons to fix the strange quark mass is negligible compared to other errors in heavy-light meson mass. We take the central value from the K meson. The numerical results for M_{0b} are listed in Table XII (full) and in Table XIII (quenched).

TABLE VI. Kinetic masses in lattice units measured from the dispersion relation in full QCD.

aM_0	$\beta=1.95$				
	$K_{val}=0.1375$	$K_{val}=0.1390$	$K_{val}=0.1400$	$K_{val}=0.1410$	$K_{val}=0.1415$
$K_{sea}=0.1375$					
2.4	3.45(4)	3.38(4)	3.34(5)	3.31(6)	3.29(6)
2.9	3.95(5)	3.88(5)	3.83(6)	3.80(7)	3.79(8)
3.4	4.43(6)	4.36(7)	4.31(8)	4.28(9)	4.28(10)
4.0	5.01(7)	4.93(9)	4.88(10)	4.85(12)	4.85(14)
4.8	5.76(10)	5.67(12)	5.62(13)	5.60(16)	5.61(19)
$K_{sea}=0.1390$					
2.4	3.41(6)	3.36(7)	3.34(9)	3.36(13)	3.42(16)
2.9	3.91(8)	3.86(10)	3.85(12)	3.90(17)	3.99(23)
3.4	4.41(10)	4.36(13)	4.35(16)	4.43(24)	4.56(32)
4.0	4.99(13)	4.94(17)	4.94(22)	5.07(33)	5.27(45)
4.8	5.75(19)	5.69(25)	5.72(32)	5.92(49)	6.25(69)
$K_{sea}=0.1400$					
2.4	3.39(5)	3.31(8)	3.28(11)	3.28(11)	3.28(14)
2.9	3.92(7)	3.83(11)	3.82(15)	3.82(15)	3.82(20)
3.4	4.44(9)	4.36(15)	4.35(21)	4.35(21)	4.38(27)
4.0	5.06(13)	4.99(21)	5.01(30)	5.01(30)	5.07(39)
4.8	6.01(21)	5.81(32)	5.89(46)	5.89(46)	6.03(62)
$K_{sea}=0.1410$					
2.4	3.22(6)	3.13(7)	3.06(9)	2.98(11)	2.99(19)
2.6	3.68(8)	3.58(9)	3.50(11)	3.51(19)	3.48(24)
2.9	4.12(9)	4.00(11)	3.91(14)	3.99(24)	3.98(30)
3.2	4.63(12)	4.49(14)	4.39(17)	4.56(31)	4.59(40)
3.5	5.27(15)	5.11(19)	4.99(23)	5.33(45)	5.42(59)
$\beta=2.1$					
aM_0	$K_{val}=0.1357$	$K_{val}=0.1367$	$K_{val}=0.1374$	$K_{val}=0.1382$	$K_{val}=0.1385$
$K_{sea}=0.1357$					
2.4	3.37(9)	3.26(14)	3.29(18)	3.39(27)	3.34(34)
2.6	3.44(13)	3.48(17)	3.51(21)	3.63(33)	3.58(41)
2.9	3.74(17)	3.80(21)	3.89(27)	4.00(43)	3.93(54)
3.2	4.04(21)	4.13(26)	4.19(34)	4.38(56)	4.28(71)
3.5	4.34(25)	4.45(33)	4.53(42)	4.78(72)	4.66(48)
$K_{sea}=0.1367$					
2.4	3.04(9)	3.03(10)	3.04(11)	3.03(14)	3.04(16)
2.6	3.23(10)	3.23(11)	3.24(13)	3.22(16)	3.24(18)
2.9	3.51(12)	3.52(14)	3.53(16)	3.52(20)	3.54(23)
3.2	3.79(14)	3.81(17)	3.83(19)	3.81(25)	3.84(27)
3.5	4.07(17)	4.09(10)	4.13(23)	4.10(30)	4.13(33)
$K_{sea}=0.1374$					
2.4	3.13(9)	3.09(11)	3.05(12)	3.00(15)	2.96(18)
2.6	3.33(11)	3.28(12)	3.24(13)	3.19(17)	3.14(20)
2.9	3.62(12)	3.56(14)	3.52(15)	3.46(21)	3.42(24)
3.2	3.91(14)	3.84(16)	3.79(18)	3.74(24)	3.70(29)
3.5	4.19(16)	4.11(18)	4.05(20)	4.01(28)	3.98(34)
$K_{sea}=0.1382$					
2.4	2.95(8)	2.93(10)	2.93(13)	2.92(18)	2.94(22)
2.6	3.12(8)	3.11(11)	3.11(14)	3.12(20)	3.13(25)
2.9	3.39(10)	3.38(13)	3.39(16)	3.40(24)	3.42(29)
3.2	3.65(11)	3.65(15)	3.67(19)	3.68(28)	3.69(34)
3.5	3.91(11)	3.92(17)	3.94(22)	3.95(32)	3.96(40)

TABLE VII. Kinetic masses in lattice units measured from the dispersion relation in the quenched case.

$\beta=2.187$					
aM_0	$K=0.1351$	$K=0.1365$	$K=0.1375$	$K=0.1385$	$K=0.1390$
2.4	3.36(8)	3.29(8)	3.26(9)	3.23(11)	3.24(12)
2.9	3.84(9)	3.79(10)	3.76(12)	3.73(14)	3.71(15)
3.4	4.33(11)	4.28(13)	4.25(15)	4.22(17)	4.21(19)
4.0	4.91(14)	4.86(17)	4.83(19)	4.82(23)	4.82(25)
4.8	5.65(19)	5.61(23)	5.60(27)	5.62(32)	5.65(35)
$\beta=2.281$					
aM_0	$K=0.1343$	$K=0.1357$	$K=0.1367$	$K=0.1377$	$K=0.1383$
2.4	3.35(7)	3.28(8)	3.22(9)	3.17(11)	3.17(14)
2.9	3.88(9)	3.79(11)	3.72(12)	3.66(15)	3.64(18)
3.4	4.40(12)	4.29(14)	4.20(16)	4.13(19)	4.10(23)
4.0	5.01(16)	4.88(18)	4.78(21)	4.67(25)	4.63(30)
4.8	5.82(23)	5.66(26)	5.51(29)	5.38(35)	5.32(41)
$\beta=2.334$					
aM_0	$K=0.1337$	$K=0.1349$	$K=0.1358$	$K=0.1368$	$K=0.1374$
2.4	3.17(7)	3.11(7)	3.08(8)	3.04(9)	3.03(11)
2.9	3.64(9)	3.58(10)	3.54(11)	3.51(12)	3.47(15)
3.4	4.10(11)	4.04(12)	4.00(14)	3.96(16)	3.90(19)
4.0	4.64(15)	4.57(16)	4.52(18)	4.41(20)	4.39(24)
4.8	5.33(20)	5.25(22)	5.19(24)	5.03(27)	5.00(32)
$\beta=2.575$					
aM_0	$K=0.1329$	$K=0.1337$	$K=0.1344$	$K=0.1351$	$K=0.1353$
2.4	2.77(09)	2.71(11)	2.65(13)	2.57(17)	2.55(19)
2.6	2.94(10)	2.87(12)	2.89(15)	2.73(19)	2.69(22)
2.9	3.18(12)	3.11(14)	3.04(18)	2.95(23)	2.91(26)
3.2	3.43(14)	3.35(17)	3.26(21)	3.17(28)	3.13(31)
3.5	3.67(16)	3.58(20)	3.49(24)	3.38(33)	3.34(36)

C. Decay constants

The decay constants are calculated from the results of the fit [Eqs. (15) and (16)] according to

$$a^{3/2}(f\sqrt{M})^{(i)} = \frac{1}{\sqrt{M}} \langle 0 | J_L^{(i)} | P(\vec{0}) \rangle = \sqrt{2} Z_L^{(i)} \sqrt{1 - \frac{3K}{4K_c}}, \quad (22)$$

where $|P(\vec{0})\rangle$ denotes a pseudoscalar heavy-light meson state of mass M at rest. The normalization factor $\sqrt{1 - (3K/4K_c)}$ for the light quark field in Eq. (22) is motivated by the mean-field improvement of the perturbative renormalization factor [22], with which the one-loop coefficient $\rho_A^{(0)}$ in Eq. (9) is modified. The lattice results for the matrix elements $(f\sqrt{M})^{(0)}$ and $(f\sqrt{M})^{(1)}$ are listed in Tables XIV and XV for full QCD and in Tables XVI–XIX for quenched QCD. As mentioned above in Sec. II B, $(f\sqrt{M})^{(2)} = (f\sqrt{M})^{(1)}$ at zero momentum.

The physical decay constant is then obtained, following Eq. (9), by

$$f\sqrt{M} = (1 + \alpha_s \rho_A^{(0)}) (f\sqrt{M})^{(0)} + (1 + \alpha_s \rho_A^{(1)}) (f\sqrt{M})^{(1)} + \alpha_s \rho_A^{(2)} (f\sqrt{M})^{(2)}. \quad (23)$$

One-loop corrections of different currents contribute with different signs and partially cancel each other. As shown in Fig. 8 as an example for full QCD, the relative contribution of each of these corrections to the whole decay matrix ele-

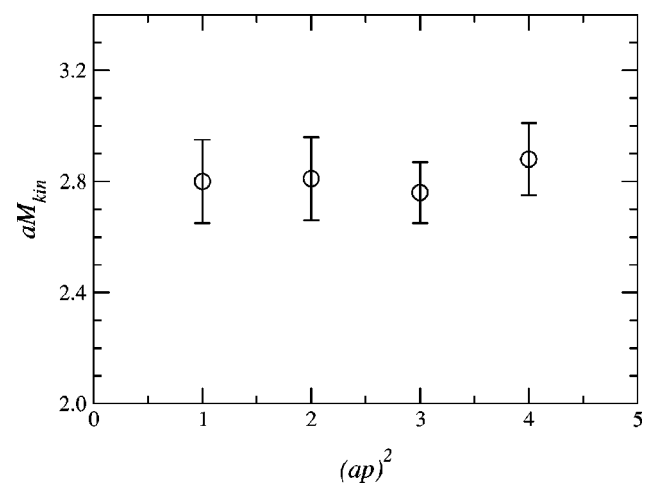


FIG. 5. Kinetic mass at $\beta=2.575$, extracted from Eq. (18), in lattice units, as a function of the momentum p^2 in units of $(2\pi/L)^2$. The quark mass parameters are $K_{sea}=0.1344$ and $aM_0=2.6$.

TABLE VIII. Simulation energies in full QCD, in lattice units.

aM^0	$\beta=1.95$				
	$K_{val}=0.1375$	$K_{val}=0.1390$	$K_{val}=0.1400$	$K_{val}=0.1410$	$K_{val}=0.1415$
$K_{sea}=0.1375$					
2.4	0.712(1)	0.679(1)	0.657(2)	0.635(2)	0.624(2)
2.9	0.730(1)	0.697(1)	0.675(2)	0.654(2)	0.643(2)
3.4	0.741(1)	0.709(2)	0.688(2)	0.667(2)	0.656(2)
4.0	0.750(1)	0.719(2)	0.698(2)	0.677(2)	0.667(2)
4.8	0.757(2)	0.727(2)	0.706(2)	0.686(2)	0.676(3)
$K_{sea}=0.1390$					
2.4	0.694(2)	0.661(2)	0.639(2)	0.617(2)	0.607(3)
2.9	0.712(2)	0.679(2)	0.658(2)	0.637(3)	0.627(3)
3.4	0.724(2)	0.692(2)	0.671(2)	0.650(3)	0.640(3)
4.0	0.734(2)	0.703(2)	0.682(2)	0.662(3)	0.652(3)
4.8	0.743(2)	0.712(2)	0.692(3)	0.672(3)	0.662(4)
$K_{sea}=0.1400$					
2.4	0.677(1)	0.641(2)	0.618(2)	0.594(2)	0.582(3)
2.9	0.694(2)	0.659(2)	0.636(2)	0.613(3)	0.601(3)
3.4	0.705(2)	0.671(2)	0.649(2)	0.626(3)	0.614(3)
4.0	0.715(2)	0.681(2)	0.659(2)	0.636(3)	0.624(3)
4.8	0.723(2)	0.690(2)	0.667(3)	0.645(3)	0.634(4)
$K_{sea}=0.1410$					
2.4	0.656(2)	0.620(2)	0.596(3)	0.573(3)	0.561(3)
2.9	0.673(2)	0.637(2)	0.614(3)	0.591(3)	0.580(4)
3.4	0.684(2)	0.649(2)	0.627(3)	0.604(3)	0.592(4)
4.0	0.693(2)	0.659(3)	0.637(3)	0.614(4)	0.603(4)
4.8	0.701(2)	0.668(3)	0.646(3)	0.624(4)	0.612(4)
$\beta=2.1$					
aM^0	$K_{val}=0.1357$	$K_{val}=0.1367$	$K_{val}=0.1374$	$K_{val}=0.1382$	$K_{val}=0.1385$
$K_{sea}=0.1357$					
2.4	0.585(2)	0.559(2)	0.540(2)	0.519(3)	0.510(3)
2.6	0.592(2)	0.566(2)	0.547(2)	0.526(3)	0.517(3)
2.9	0.600(2)	0.574(2)	0.555(2)	0.534(3)	0.526(3)
3.2	0.606(2)	0.580(2)	0.562(2)	0.541(3)	0.532(3)
3.5	0.611(2)	0.585(2)	0.567(2)	0.546(3)	0.538(3)
$K_{sea}=0.1367$					
2.4	0.575(2)	0.548(2)	0.529(2)	0.507(3)	0.499(3)
2.6	0.582(2)	0.555(2)	0.536(2)	0.514(3)	0.506(3)
2.9	0.590(2)	0.563(2)	0.544(2)	0.523(3)	0.515(3)
3.2	0.596(2)	0.570(2)	0.551(2)	0.530(3)	0.522(3)
3.5	0.601(2)	0.575(2)	0.556(3)	0.536(3)	0.528(4)
$K_{sea}=0.1374$					
2.4	0.564(2)	0.536(2)	0.516(2)	0.494(3)	0.485(3)
2.6	0.570(2)	0.542(2)	0.523(2)	0.500(3)	0.492(3)
2.9	0.578(2)	0.550(2)	0.531(2)	0.509(3)	0.500(3)
3.2	0.584(2)	0.557(2)	0.538(2)	0.515(3)	0.507(3)
3.5	0.589(2)	0.562(2)	0.543(2)	0.521(3)	0.512(3)
$K_{sea}=0.1382$					
2.4	0.553(2)	0.524(2)	0.505(3)	0.483(3)	0.476(4)
2.6	0.559(2)	0.531(2)	0.511(3)	0.490(3)	0.483(4)
2.9	0.567(2)	0.539(3)	0.519(3)	0.498(3)	0.491(4)
3.2	0.574(2)	0.546(3)	0.526(3)	0.505(3)	0.498(4)
3.5	0.579(2)	0.551(3)	0.532(3)	0.510(4)	0.503(4)

TABLE IX. Quenched simulation energies, in lattice units.

$\beta=2.187$					
aM_0	$K=0.1351$	$K=0.1365$	$K=0.1375$	$K=0.1385$	$K=0.1390$
2.4	0.707(2)	0.675(2)	0.652(3)	0.629(3)	0.617(3)
2.6	0.724(2)	0.693(2)	0.671(3)	0.649(3)	0.637(4)
2.9	0.736(2)	0.706(2)	0.684(3)	0.662(3)	0.651(4)
3.2	0.746(2)	0.716(3)	0.694(3)	0.673(3)	0.662(4)
3.5	0.754(2)	0.725(3)	0.704(3)	0.683(3)	0.672(4)
$\beta=2.281$					
aM_0	$K=0.1343$	$K=0.1357$	$K=0.1367$	$K=0.1377$	$K=0.1383$
2.4	0.648(2)	0.614(3)	0.590(3)	0.566(4)	0.551(4)
2.9	0.664(3)	0.631(3)	0.608(3)	0.584(4)	0.569(5)
3.4	0.674(3)	0.642(3)	0.619(4)	0.597(5)	0.582(5)
4.0	0.683(3)	0.652(3)	0.629(4)	0.607(5)	0.593(5)
4.8	0.691(3)	0.660(3)	0.639(4)	0.617(5)	0.604(5)
$\beta=2.334$					
aM_0	$K=0.1337$	$K=0.1349$	$K=0.1358$	$K=0.1368$	$K=0.1374$
2.4	0.623(2)	0.592(3)	0.569(3)	0.544(4)	0.529(5)
2.9	0.638(2)	0.608(3)	0.586(3)	0.561(4)	0.546(5)
3.4	0.648(2)	0.619(3)	0.597(3)	0.572(4)	0.558(5)
4.0	0.657(3)	0.628(3)	0.606(3)	0.582(4)	0.568(5)
4.8	0.665(3)	0.636(3)	0.615(4)	0.591(5)	0.577(6)
$\beta=2.575$					
aM_0	$K=0.1329$	$K=0.1337$	$K=0.1344$	$K=0.1351$	$K=0.1353$
2.4	0.501(2)	0.478(2)	0.459(2)	0.440(3)	0.435(3)
2.9	0.506(2)	0.484(2)	0.464(3)	0.446(3)	0.441(3)
3.4	0.513(2)	0.491(2)	0.472(3)	0.454(3)	0.449(4)
4.0	0.518(2)	0.496(2)	0.478(3)	0.460(3)	0.455(4)
4.8	0.523(2)	0.501(2)	0.482(3)	0.465(3)	0.460(4)

ment $f\sqrt{M}$ is small. The largest is the correction to $(f\sqrt{M})^{(0)}$, being of the order of a few percent. The overall one-loop correction is 3–6% for the dynamical case, and 3–5% for the quenched case. The one-loop correction for the RG-improved gauge action is thus smaller than for the plaquette gauge action for which the correction amounts to roughly 10% (see e.g., Refs. [14,15]).

D. Analysis of heavy and light quark mass dependence

We find that the decay matrix elements $a^{3/2}(f\sqrt{M})^{(i)}$ are well described by a linear function in the light quark mass $1/(2K) - 1/(2K_c)$ as shown in Fig. 9 (top panel). Using the linear fit, we interpolate the data to K_s or extrapolate to K_l . Then we make a quadratic fit in $1/M_0$ and interpolate to the b quark mass, $1/M_{0b}$. Figure 9 (bottom) shows this fit for full QCD on the finest lattice.

For quenched QCD this completes the analysis of the decay constant. We give the renormalized decay constants in Table XX.

For full QCD we carry out this procedure separately for each sea quark mass m_{sea} , using partially quenched values for the lattice spacing and K_c , K_l and K_s . The resulting renormalized decay constants are given in Table XXI. From

these data we calculate the physical decay constants by extrapolating the sea quark mass to the u and d quark masses. We use a linear fit in $(am_\pi)^2$, where m_π is the pion mass of the sea quark. The sea quark mass dependence of f_B , f_{B_s} , and f_{B_s}/f_B is very mild. On finer lattices, there is a slight upward shift of the decay constants as the sea quark mass is decreased. In Fig. 10, this is demonstrated for f_B at $\beta=2.1$. The final results for full QCD are given in Table XXII. We note that the decay constants we obtained for finite lattice spacings agree very well with those from the Fermilab formalism [5] for both quenched and full calculations.

We add comments on possible systematic errors from various steps of the analysis procedure: (i) The bare b quark mass using the ρ mass to set the scale is slightly higher than that from the Y , but the two agree within statistical errors. (ii) The statistical error on the mass is included within the bootstrap procedure. There is a good agreement between results from M_{kin} and M_{pert} ; if the perturbative error is included in the determination using M_{pert} , their errors are very similar. We take results obtained with the kinetic masses for our central values. (iii) An alternative method to represent the heavy quark dependence of $f^{(i)}\sqrt{M}$ is to employ the heavy-light meson mass instead of the heavy quark mass.

TABLE X. Meson masses with the perturbative mass shifts in full QCD, in lattice units.

aM_0	$\beta=1.95$				
	$K_{val}=0.1375$	$K_{val}=0.1390$	$K_{val}=0.1400$	$K_{val}=0.1410$	$K_{val}=0.1415$
$K_{sea}=0.1375$					
2.4	3.08(15)	3.04(15)	3.02(15)	3.00(15)	2.99(15)
2.9	3.64(18)	3.60(18)	3.58(18)	3.56(18)	3.55(18)
3.4	4.18(21)	4.15(21)	4.13(21)	4.11(21)	4.10(21)
4.0	4.83(24)	4.80(24)	4.78(24)	4.76(24)	4.75(24)
4.8	5.69(28)	5.66(28)	5.64(28)	5.62(28)	5.61(28)
$K_{sea}=0.1390$					
2.4	3.06(15)	3.02(15)	3.00(15)	2.98(15)	2.97(15)
2.9	3.62(18)	3.59(18)	3.56(18)	3.54(18)	3.53(18)
3.4	4.17(21)	4.14(21)	4.11(21)	4.09(20)	4.08(20)
4.0	4.82(24)	4.79(24)	4.76(24)	4.74(24)	4.73(24)
4.8	5.67(28)	5.64(28)	5.62(28)	5.60(28)	5.59(28)
$K_{sea}=0.1400$					
2.4	3.04(15)	3.00(15)	2.98(15)	2.96(15)	2.95(15)
2.9	3.60(18)	3.57(18)	3.54(18)	3.52(18)	3.51(18)
3.4	4.15(21)	4.12(21)	4.09(20)	4.07(20)	4.06(20)
4.0	4.80(24)	4.76(24)	4.74(24)	4.72(24)	4.71(24)
4.8	5.65(28)	5.62(28)	5.60(28)	5.57(28)	5.56(28)
$K_{sea}=0.1410$					
2.4	3.02(15)	2.98(15)	2.96(15)	2.94(15)	2.92(15)
2.6	3.58(18)	3.54(18)	3.52(18)	3.50(18)	3.49(17)
2.9	4.13(21)	4.09(20)	4.07(20)	4.05(20)	4.04(20)
3.2	4.78(24)	4.74(24)	4.72(24)	4.70(24)	4.69(23)
3.5	5.63(28)	5.60(28)	5.58(28)	5.55(28)	5.54(28)
$\beta=2.1$					
aM_0	$K_{val}=0.1357$	$K_{val}=0.1367$	$K_{val}=0.1374$	$K_{val}=0.1382$	$K_{val}=0.1385$
$K_{sea}=0.1357$					
2.4	2.95(12)	2.93(12)	2.91(12)	2.89(12)	2.88(12)
2.6	3.18(13)	3.15(13)	3.13(13)	3.11(12)	3.10(12)
2.9	3.51(14)	3.48(14)	3.46(14)	3.44(14)	3.43(14)
3.2	3.83(15)	3.81(15)	3.79(15)	3.77(15)	3.76(15)
3.5	4.16(17)	4.13(17)	4.11(16)	4.09(16)	4.08(16)
$K_{sea}=0.1367$					
2.4	2.94(12)	2.91(12)	2.90(12)	2.87(12)	2.87(12)
2.6	3.17(13)	3.14(13)	3.12(12)	3.10(12)	3.09(12)
2.9	3.50(14)	3.47(14)	3.45(14)	3.43(14)	3.42(14)
3.2	3.82(15)	3.80(15)	3.78(15)	3.76(15)	3.75(15)
3.5	4.15(17)	4.12(16)	4.10(16)	4.08(16)	4.07(16)
$K_{sea}=0.1374$					
2.4	2.93(12)	2.90(12)	2.88(12)	2.86(11)	2.85(11)
2.6	3.15(13)	3.13(13)	3.11(12)	3.08(12)	3.08(12)
2.9	3.48(14)	3.46(14)	3.44(14)	3.41(14)	3.41(14)
3.2	3.81(15)	3.78(15)	3.76(15)	3.74(15)	3.73(15)
3.5	4.14(17)	4.11(16)	4.09(16)	4.07(16)	4.06(16)
$K_{sea}=0.1382$					
2.4	2.92(12)	2.89(12)	2.87(11)	2.85(11)	2.84(11)
2.6	3.14(13)	3.11(12)	3.09(12)	3.07(12)	3.07(12)
2.9	3.47(14)	3.44(14)	3.43(14)	3.40(14)	3.40(14)
3.2	3.80(15)	3.77(15)	3.75(15)	3.73(15)	3.72(15)
3.5	4.13(17)	4.10(16)	4.08(16)	4.06(16)	4.05(16)

TABLE XI. Quenched meson masses with perturbative mass shifts, in lattice units.

aM_0	$\beta=2.187$				
	$K=0.1351$	$K=0.1365$	$K=0.1375$	$K=0.1385$	$K=0.1390$
2.4	3.07(15)	3.04(15)	3.02(15)	2.99(15)	2.98(15)
2.9	3.63(18)	3.60(18)	3.58(18)	3.55(18)	3.54(18)
3.4	4.18(21)	4.15(21)	4.13(21)	4.11(21)	4.09(20)
4.0	4.83(24)	4.80(24)	4.78(24)	4.76(24)	4.75(24)
4.8	5.68(28)	5.65(28)	5.63(28)	5.61(28)	5.60(28)
$\beta=2.281$					
aM_0	$K=0.1343$	$K=0.1357$	$K=0.1367$	$K=0.1377$	$K=0.1383$
2.4	3.01(15)	2.98(15)	2.96(15)	2.93(15)	2.92(15)
2.9	3.57(18)	3.54(18)	3.51(18)	3.49(17)	3.48(17)
3.4	4.12(21)	4.08(20)	4.06(20)	4.04(20)	4.02(20)
4.0	4.76(24)	4.73(24)	4.71(24)	4.69(23)	4.67(23)
4.8	5.61(28)	5.58(28)	5.56(28)	5.54(28)	5.53(28)
$\beta=2.334$					
aM_0	$K=0.1337$	$K=0.1349$	$K=0.1358$	$K=0.1368$	$K=0.1374$
2.4	2.99(12)	2.96(12)	2.94(12)	2.91(12)	2.90(12)
2.9	3.54(14)	3.51(14)	3.49(14)	3.47(14)	3.45(14)
3.4	4.09(16)	4.06(16)	4.04(16)	4.01(16)	4.00(16)
4.0	4.73(19)	4.70(19)	4.68(19)	4.66(19)	4.64(19)
4.8	5.58(22)	5.56(22)	5.53(22)	5.51(22)	5.50(22)
$\beta=2.575$					
aM_0	$K=0.1329$	$K=0.1337$	$K=0.1344$	$K=0.1351$	$K=0.1353$
2.4	2.87(9)	2.85(9)	2.83(8)	2.81(8)	2.81(8)
2.6	3.09(9)	3.07(9)	3.05(9)	3.03(9)	3.03(9)
2.9	3.42(10)	3.40(10)	3.38(10)	3.36(10)	3.36(10)
3.2	3.75(11)	3.72(11)	3.70(11)	3.69(11)	3.68(12)
3.5	4.07(12)	4.05(12)	4.03(12)	4.01(12)	4.00(12)

This circumvents the determination of M_{0b} . The results agree with those using M_{0b} within the statistical errors, which are similar in magnitude in both methods. We quote the numbers from the procedure using M_{0b} as our central values.

V. ESTIMATE OF CONTINUUM RESULTS

While discretization errors decrease as the lattice spacing becomes smaller, the $1/M$ operators introduce radiative corrections that go as powers of $1/a$ in NRQCD. Thus NRQCD breaks down in the limit of vanishing lattice spacing, and we cannot perform a continuum extrapolation as a matter of principle. The aim is rather to find a range of lattice spacings where the result is approximately independent of the cutoff with small systematic errors.

We have plotted the resulting f_B and f_{B_s} at finite lattice spacing in Figs. 11 and 12 for both quenched and full QCD calculations, where statistical errors are shown by thick bar symbols. We see that the data for quenched QCD (top panels) exhibit a signature for a plateau for $a_\rho \leq 0.8 \text{ GeV}^{-1}$. The data for full QCD calculation, however, show a sizable drop from $a_\rho = 0.79$ to 0.56 GeV^{-1} . Nevertheless, it is perhaps possible to estimate the continuum value if we can properly

estimate the discretization error at each lattice spacing, and we consider this problem in the following.

The leading systematic errors due to finite lattice spacings are $O(\alpha_s a \Lambda_{QCD})$ and $O(a^2 \Lambda_{QCD}^2)$ with the clover action for light valence quarks. In the NRQCD heavy quark action, the tree level matching of the chromomagnetic coupling c_B leads to an error of $O(\alpha_s \Lambda_{QCD}/M_b)$. We also expect the discretization error of $O(\Lambda_{QCD}/M_b)$ from the NRQCD action. Since the matching calculation of the axial current has been made in one-loop perturbation theory, we expect an $O(\alpha_s^2)$ radiative correction. In addition, there is an $O[\alpha_s^2/(aM_b)]$ term, which is formally subleading compared to the $O(\alpha_s^2)$ term, but still gives one of the leading $1/a$ contributions. An $O(\Lambda_{QCD}^2/M_b^2)$ contribution comes from the neglected $1/M^2$ corrections to the NRQCD Lagrangian. In Table XXIII we list an estimate of the systematic errors for f_B and f_{B_s} on our lattices. We use $\alpha_{\overline{\text{MS}}}(1/a)$ for the coupling constant α_s . For the typical momentum scale Λ_{QCD} , we naively expect that its order is around 200–300 MeV. In this analysis, however, we take a value which is larger by a factor 2 and use $\Lambda_{QCD}=600 \text{ MeV}$, in order to make the estimate more conservative. The overall error is calculated by summing the individual contributions in quadrature.

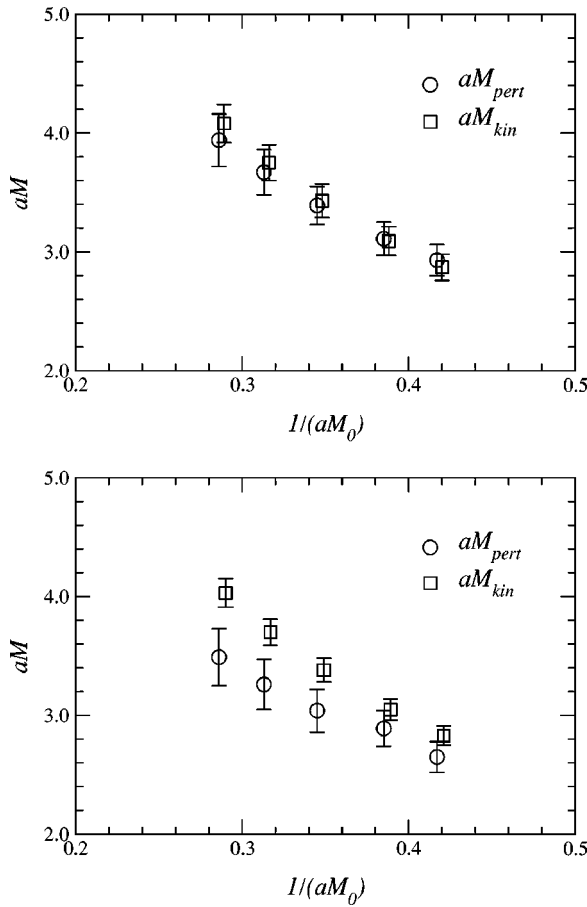


FIG. 6. Comparison of kinetic mass (circles) and mass using perturbative shifts (squares) in full QCD at $\beta=2.1$, $K_{sea}=0.1382$ and $K_{val}=0.1374$ (top panel), and in quenched QCD at $\beta=2.575$ and $K=0.1344$ (bottom panel).

TABLE XII. Bare b quark masses M_{0b} , in GeV, for the full QCD lattices. Results with two different scale determinations m_ρ and Y are listed for each sea quark mass.

β	K_{sea}	Scale from ρ	Scale from Y
1.95	0.1375	4.53(12)	4.43(13)
	0.1390	4.29(26)	4.14(28)
	0.1400	4.26(21)	4.18(23)
	0.1410	4.88(23)	4.77(23)
	0.1357	4.08(34)	3.95(30)
2.1	0.1367	4.45(24)	
	0.1374	4.41(25)	
	0.1382	4.65(42)	4.44(43)

In Figs. 11 and 12 the discretization errors thus estimated are shown with thin error bars. Looking first at figures for the quenched case (top panels) we see that the ranges of error bars overlap among all data points, but also that the value of plateau is within the ranges of error bars. Therefore, we consider that the continuum value of the quenched decay constant is located within the estimated errors. We take the data at the weakest coupling, with which the error estimate becomes minimum,

$$f_B^{N_f=0} = 191 \pm 4 \pm 27 \text{ MeV}, \quad (24)$$

$$f_{B_s}^{N_f=0} = 220 \pm 4 \pm 31 \text{ MeV}, \quad (25)$$

as our estimate for the continuum value, where the first error is statistical, and the second is the uncertainty associated with the discretization. These values are shown by horizontal lines in the figure. The errors here do not include systematic errors from the uncertainties of the strange quark mass (3%) and the lattice scale which exceeds 30% (see Fig. 4). The error due to strange quark mass is ascribed to both lattice

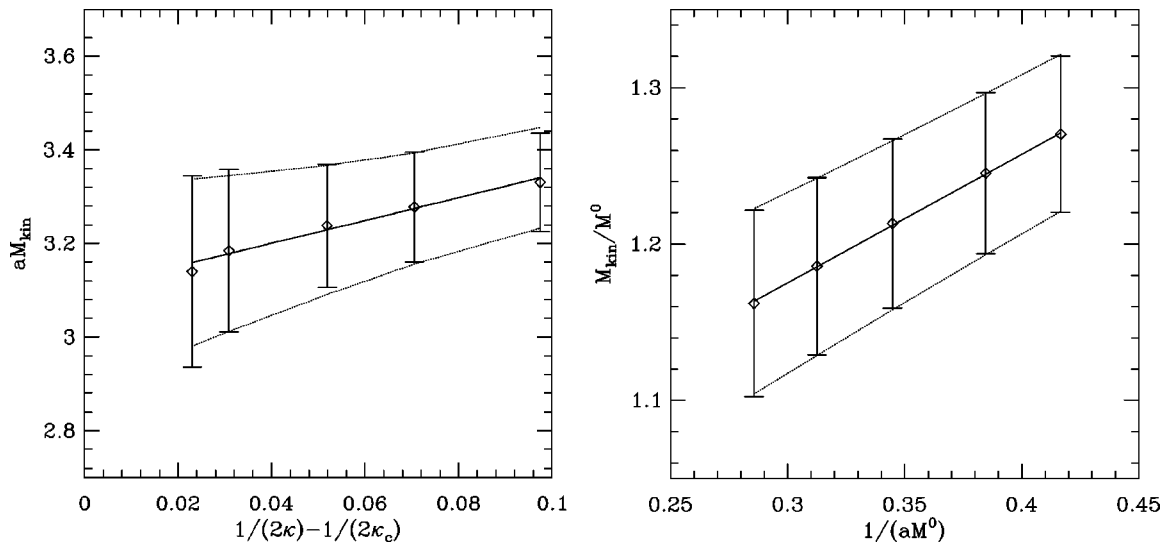


FIG. 7. Kinetic meson mass for the parameter values $\beta=2.1$ and $K_{sea}=0.1374$ in full QCD. The left panel shows a fit of M_{kin} as a function of the light quark mass for $aM_0=2.6$, which is close to M_{0b} . The right panel shows a fit in the heavy quark mass with the light quark mass interpolated to the strange quark mass. Solid lines denote the fits and dashed lines the error.

TABLE XIII. Bare b quark masses M_{0b} , in GeV, for the quenched lattices. Results with two different scale determinations m_ρ and Υ are listed for each sea quark mass.

β	Scale from ρ	Scale from Υ
2.187	4.55(24)	4.42(25)
2.281	4.45(23)	4.32(24)
2.334	4.54(27)	
2.575	5.15(39)	

artifacts and quenching effects. As seen in Table XX this uncertainty decreases toward weaker couplings. On the other hand, the uncertainty due to lattice scale does not diminish from strong to weaker couplings.

For the full QCD case, we could not see a plateau within the statistical errors in Figs. 11 and 12. From the same reasoning as in the quenched case, however, we expect that the continuum value is within the error range when we include systematic errors. Indeed, the final error bars of the two data points largely overlap in Figs. 11 and 12. Taking the data with a smaller error bar (i.e., at the weaker coupling), we have

$$f_B^{N_f=2} = 204 \pm 8 \pm 29 \text{ MeV}, \quad (26)$$

$$f_{B_s}^{N_f=2} = 242 \pm 9 \pm 34 \text{ MeV} \quad (27)$$

as our “final” estimate. We take these values as still provisional, since a plateau is not identified within the statistical errors. In full QCD, the uncertainty from the strange quark mass is about 1%. The uncertainty from the lattice scale is 22% in full QCD, which is smaller than that in the quenched case, but is still substantial (see Fig. 13). To be conservative we add this error to the final estimate of errors for the decay constants.

Figure 14 shows a similar analysis for the ratio f_{B_s}/f_B . This ratio is rather insensitive to the perturbative corrections and the heavy quark action. The dominant errors come from the light quark action, i.e., $O(\alpha_s a \Lambda_{QCD})$ and $O(a^2 \Lambda_{QCD}^2)$. We estimate the systematic error of $f_{B_s}/f_B - 1$ by quadrature. We again find the systematic error to be smallest at the finest lattice spacing, whose results are therefore taken as our final estimates. We obtain

$$\left(\frac{f_{B_s}}{f_B} \right)^{N_f=0} = 1.150 \pm 0.009 \pm 0.020, \quad (28)$$

$$\left(\frac{f_{B_s}}{f_B} \right)^{N_f=2} = 1.179 \pm 0.018 \pm 0.023. \quad (29)$$

To study the effect of dynamical sea quarks, we take the ratio of unquenched results to quenched results. We expect that most systematic errors cancel, and we obtain

$$\frac{f_B^{N_f=2}}{f_B^{N_f=0}} = 1.07(5), \quad (30)$$

$$\frac{f_{B_s}^{N_f=2}}{f_{B_s}^{N_f=0}} = 1.10(5), \quad (31)$$

$$\frac{(f_{B_s}/f_B)^{N_f=2}}{(f_{B_s}/f_B)^{N_f=0}} = 1.03(2), \quad (32)$$

where only the statistical errors are retained. We observe that the inclusion of dynamical sea quarks increases the decay constants, as noted in Refs. [6,7]. The effects are 1.5σ for f_B , and 2σ for f_{B_s} .

VI. COMPARISON WITH OTHER STUDIES

We first note that the decay constants we obtained with the NRQCD formalism agree very well with those obtained using the Fermilab formalism: $f_B = 188 \pm 3 \pm 26$ MeV and $f_{B_s} = 220 \pm 2 \pm 31$ MeV from a quenched calculation, and $f_B = 208 \pm 10 \pm 29$ MeV and $f_{B_s} = 250 \pm 10 \pm 35$ MeV from a full QCD calculation [5]. This justifies the validity of the two formalisms within the statistical and systematic errors.

We now compare our quenched calculation to the previous NRQCD results (Refs. [14] and [15]), and to a quenched world average [1] in Fig. 15. In Ref. [14], marked as GLOK in Fig. 15, the clover light quark action is used with a tree-level mean-field-improved clover coefficient, and the NRQCD action includes $1/M^2$ corrections at the tree level. The lattice spacing, fixed from m_ρ , is $a^{-1} = 2$ GeV. The calculation of the JLQCD Collaboration [15] employed the clover light quark action with a mean-field-improved one-loop clover coefficient, and heavy quarks with NRQCD corrected through $O(1/M)$. The scaling of the decay constant is tested at three lattice spacings, and the central value is extracted from runs at a lattice spacing $a^{-1} \approx 1.6$ GeV, with the string tension used to set the scale. The scaling test is also made for f_{B_s} in Ref. [24] in the range $a^{-1} = 1.1 - 2.6$ GeV. For the world average, we use the value quoted in Ref. [1] that includes a variety of quark actions. Our value (labeled as “this work”) is slightly higher than those of JLQCD and the world average by 1.5σ . Our value, however, disagrees with the GLOK result by $(2.5 - 3)\sigma$.

In Fig. 16, we compare our result from two-flavor QCD with other dynamical calculations that use the plaquette gauge action. Reference [6], denoted as SGO, uses the NRQCD action corrected through $O(1/M)$ for the heavy quark and a tree-level clover action for the light valence quark. The calculation used a set of dynamical gauge configurations with staggered quarks at a mass around the strange quark mass, but on a somewhat small physical volume ($L_s \sim 1.6$ fm). The lattice spacing ($a^{-1} \approx 2$ GeV) is fixed with m_ρ . The result from MILC [7] is an ongoing study using two flavors of staggered sea quarks, and both Wilson and (fat-link) clover action for valence quarks. The lattice spacings are set using f_π , and the central value is extracted from the continuum extrapolation of the Wilson results. Our result is again slightly higher, but agrees with the others within one sigma error.

TABLE XIV. Decay matrix elements at $\beta=1.95$.

aM_0	$a^{3/2}(f\sqrt{M})^{(0)}$				
	$K_{val}=0.1375$	$K_{val}=0.1390$	$K_{val}=0.1400$	$K_{val}=0.1410$	$K_{val}=0.1415$
$K_{sea}=0.1375$					
2.4	0.567(5)	0.576(5)	0.595(4)	0.613(4)	0.640(4)
2.9	0.595(6)	0.606(5)	0.626(5)	0.646(4)	0.676(4)
3.4	0.619(6)	0.630(6)	0.652(5)	0.674(5)	0.705(5)
4.0	0.643(7)	0.655(6)	0.678(6)	0.702(5)	0.736(5)
4.8	0.669(7)	0.682(7)	0.707(6)	0.732(6)	0.768(6)
$K_{sea}=0.1390$					
2.4	0.534(7)	0.543(6)	0.561(5)	0.579(5)	0.606(5)
2.9	0.561(7)	0.571(7)	0.591(6)	0.611(6)	0.640(5)
3.4	0.586(10)	0.597(9)	0.619(8)	0.641(7)	0.673(7)
4.0	0.612(11)	0.623(10)	0.646(9)	0.670(8)	0.704(7)
4.8	0.641(13)	0.653(11)	0.678(10)	0.702(09)	0.739(8)
$K_{sea}=0.1400$					
2.4	0.484(6)	0.496(5)	0.518(4)	0.539(4)	0.570(4)
2.9	0.508(6)	0.520(6)	0.544(5)	0.567(5)	0.600(4)
3.4	0.527(7)	0.540(6)	0.566(5)	0.590(5)	0.626(5)
4.0	0.546(8)	0.560(7)	0.588(6)	0.614(5)	0.652(5)
4.8	0.567(9)	0.582(8)	0.612(7)	0.640(6)	0.680(6)
$K_{sea}=0.1410$					
2.4	0.429(7)	0.441(6)	0.462(5)	0.484(5)	0.514(5)
2.9	0.449(9)	0.462(7)	0.486(6)	0.509(6)	0.542(5)
3.4	0.465(9)	0.479(8)	0.505(7)	0.530(6)	0.565(6)
4.0	0.482(11)	0.497(9)	0.525(8)	0.551(7)	0.587(6)
4.8	0.501(12)	0.517(10)	0.546(8)	0.573(8)	0.612(7)
$a^{3/2}(f\sqrt{M})^{(1)}$					
aM_0	$K_{val}=0.1375$	$K_{val}=0.1390$	$K_{val}=0.1400$	$K_{val}=0.1410$	$K_{val}=0.1415$
$K_{sea}=0.1375$					
2.4	-0.0817(12)	-0.0823(12)	-0.0836(10)	-0.0850(10)	-0.0869(9)
2.9	-0.0730(12)	-0.0735(11)	-0.0748(10)	-0.0761(9)	-0.0779(8)
3.4	-0.0661(11)	-0.0666(11)	-0.0677(9)	-0.0689(9)	-0.0706(8)
4.0	-0.0594(11)	-0.0599(10)	-0.0609(9)	-0.0620(8)	-0.0636(7)
4.8	-0.0524(10)	-0.0528(9)	-0.0538(8)	-0.0547(8)	-0.0562(7)
$K_{sea}=0.1390$					
2.4	-0.0754(11)	-0.0761(10)	-0.0775(9)	-0.0789(8)	-0.0810(8)
2.9	-0.0672(10)	-0.0678(9)	-0.0691(8)	-0.0705(8)	-0.0724(7)
3.4	-0.0614(11)	-0.0619(10)	-0.0631(9)	-0.0643(8)	-0.0662(7)
4.0	-0.0552(11)	-0.0557(10)	-0.0568(9)	-0.0580(8)	-0.0597(7)
4.8	-0.0488(11)	-0.0493(10)	-0.0503(9)	-0.0514(8)	-0.0530(7)
$K_{sea}=0.1400$					
2.4	-0.0681(8)	-0.0692(8)	-0.0712(7)	-0.0730(6)	-0.0755(6)
2.9	-0.0604(8)	-0.0614(7)	-0.0633(6)	-0.0650(6)	-0.0674(5)
3.4	-0.0544(8)	-0.0553(7)	-0.0570(6)	-0.0587(5)	-0.0609(5)
4.0	-0.0486(8)	-0.0494(7)	-0.0510(6)	-0.0525(5)	-0.0546(5)
4.8	-0.0425(7)	-0.0433(6)	-0.0447(5)	-0.0461(5)	-0.0481(5)
$K_{sea}=0.1410$					
2.4	-0.0607(12)	-0.0616(10)	-0.0637(8)	-0.0656(8)	-0.0682(7)
2.9	-0.0537(12)	-0.0545(10)	-0.0565(8)	-0.0583(7)	-0.0607(7)
3.4	-0.0482(11)	-0.0490(9)	-0.0508(8)	-0.0525(7)	-0.0547(6)
4.0	-0.0430(10)	-0.0437(9)	-0.0453(7)	-0.0469(7)	-0.0490(6)
4.8	-0.0376(10)	-0.0382(8)	-0.0397(7)	-0.0411(6)	-0.0430(6)

TABLE XV. Decay matrix elements at $\beta=2.1$.

aM_0	$K_{val}=0.1357$	$K_{val}=0.1367$	$K_{val}=0.1374$	$K_{val}=0.1382$	$K_{val}=0.1385$
$a^{3/2}(f\sqrt{M})^{(0)}$					
			$K_{sea}=0.1357$		
2.4	0.317(5)	0.324(4)	0.341(4)	0.355(4)	0.376(4)
2.6	0.322(5)	0.329(4)	0.346(4)	0.361(4)	0.383(4)
2.9	0.328(5)	0.336(4)	0.354(4)	0.369(4)	0.392(4)
3.2	0.334(5)	0.342(4)	0.360(4)	0.376(4)	0.399(4)
3.5	0.339(5)	0.347(4)	0.366(4)	0.382(4)	0.406(4)
			$K_{sea}=0.1367$		
2.4	0.299(5)	0.306(5)	0.324(4)	0.339(4)	0.360(3)
2.6	0.304(5)	0.311(5)	0.329(4)	0.345(4)	0.366(4)
2.9	0.311(5)	0.318(5)	0.337(4)	0.353(4)	0.375(4)
3.2	0.317(6)	0.324(5)	0.343(4)	0.359(4)	0.382(4)
3.5	0.322(6)	0.329(5)	0.348(5)	0.365(4)	0.389(4)
			$K_{sea}=0.1374$		
2.4	0.275(4)	0.282(4)	0.300(3)	0.316(3)	0.337(4)
2.6	0.278(4)	0.286(4)	0.305(4)	0.321(4)	0.342(4)
2.9	0.284(4)	0.291(4)	0.311(4)	0.327(4)	0.350(4)
3.2	0.288(5)	0.296(4)	0.316(4)	0.333(4)	0.356(4)
3.5	0.292(5)	0.300(5)	0.321(4)	0.338(4)	0.362(4)
			$K_{sea}=0.1382$		
2.4	0.256(5)	0.262(5)	0.281(4)	0.298(4)	0.320(4)
2.6	0.260(6)	0.266(5)	0.285(5)	0.302(4)	0.325(4)
2.9	0.265(6)	0.271(5)	0.291(5)	0.309(5)	0.332(4)
3.2	0.269(6)	0.276(6)	0.296(5)	0.315(5)	0.339(5)
3.5	0.272(7)	0.280(6)	0.301(5)	0.320(5)	0.345(5)
$a^{3/2}(f\sqrt{M})^{(1)}$					
aM_0	$K_{val}=0.1357$	$K_{val}=0.1367$	$K_{val}=0.1374$	$K_{val}=0.1382$	$K_{val}=0.1385$
			$K_{sea}=0.1357$		
2.4	-0.0381(6)	-0.0387(6)	-0.0403(5)	-0.0416(5)	-0.0435(4)
2.6	-0.0361(6)	-0.0367(5)	-0.0382(5)	-0.0395(5)	-0.0413(4)
2.9	-0.0335(6)	-0.0341(5)	-0.0355(5)	-0.0367(4)	-0.0385(4)
3.2	-0.0312(5)	-0.0318(5)	-0.0332(4)	-0.0343(4)	-0.0360(4)
3.5	-0.0293(5)	-0.0298(4)	-0.0312(4)	-0.0322(4)	-0.0338(4)
			$K_{sea}=0.1367$		
2.4	-0.0356(7)	-0.0363(6)	-0.0379(5)	-0.0393(5)	-0.0412(4)
2.6	-0.0338(6)	-0.0344(6)	-0.0360(5)	-0.0373(5)	-0.0392(4)
2.9	-0.0314(6)	-0.0319(6)	-0.0334(5)	-0.0347(5)	-0.0364(4)
3.2	-0.0292(6)	-0.0298(5)	-0.0312(5)	-0.0324(4)	-0.0341(4)
3.5	-0.0274(5)	-0.0279(5)	-0.0293(5)	-0.0304(4)	-0.0320(4)
			$K_{sea}=0.1374$		
2.4	-0.0322(5)	-0.0329(5)	-0.0346(4)	-0.0361(4)	-0.0381(4)
2.6	-0.0305(5)	-0.0311(5)	-0.0328(4)	-0.0342(4)	-0.0361(4)
2.9	-0.0283(5)	-0.0288(4)	-0.0304(4)	-0.0318(4)	-0.0336(4)
3.2	-0.0263(5)	-0.0268(4)	-0.0283(4)	-0.0296(4)	-0.0313(4)
3.5	-0.0246(4)	-0.0251(4)	-0.0265(4)	-0.0277(3)	-0.0294(3)
			$K_{sea}=0.1382$		
2.4	-0.0300(8)	-0.0306(7)	-0.0322(6)	-0.0337(5)	-0.0359(5)
2.6	-0.0284(7)	-0.0289(6)	-0.0305(5)	-0.0320(5)	-0.0341(5)
2.9	-0.0263(7)	-0.0268(6)	-0.0283(5)	-0.0297(5)	-0.0317(5)
3.2	-0.0245(7)	-0.0250(6)	-0.0264(5)	-0.0278(5)	-0.0296(5)
3.5	-0.0229(6)	-0.0234(6)	-0.0247(5)	-0.0261(5)	-0.0278(5)

TABLE XVI. Decay matrix elements at $\beta=2.187$.

	$K=0.1351$	$K=0.1365$	$K=0.1375$	$K=0.1385$	$K=0.1390$
aM_0			$a^{3/2}(f\sqrt{M})^{(0)}$		
2.4	0.539(6)	0.548(6)	0.566(5)	0.583(5)	0.607(5)
2.9	0.566(7)	0.575(6)	0.594(6)	0.613(6)	0.639(5)
3.4	0.588(7)	0.598(7)	0.618(6)	0.638(6)	0.665(5)
4.0	0.610(7)	0.621(7)	0.642(7)	0.663(6)	0.692(6)
4.8	0.634(8)	0.646(7)	0.668(7)	0.690(7)	0.721(6)
aM_0			$a^{3/2}(f\sqrt{M})^{(1)}$		
2.4	-0.0744(11)	-0.0748(10)	-0.0761(9)	-0.0772(9)	-0.0786(8)
2.9	-0.0661(10)	-0.0665(10)	-0.0678(8)	-0.0689(7)	-0.0702(7)
3.4	-0.0595(10)	-0.0599(9)	-0.0611(8)	-0.0622(7)	-0.0634(6)
4.0	-0.0531(9)	-0.0535(8)	-0.0546(7)	-0.0557(6)	-0.0570(6)
4.8	-0.0464(8)	-0.0468(8)	-0.0478(7)	-0.0488(6)	-0.0501(5)

TABLE XVII. Decay matrix elements at $\beta=2.281$.

	$K=0.1343$	$K=0.1357$	$K=0.1367$	$K=0.1377$	$K=0.1383$
aM_0			$a^{3/2}(f\sqrt{M})^{(0)}$		
2.4	0.418(7)	0.430(8)	0.448(7)	0.466(6)	0.493(6)
2.9	0.435(8)	0.448(8)	0.467(7)	0.486(7)	0.514(7)
3.4	0.450(8)	0.463(9)	0.483(8)	0.502(7)	0.532(7)
4.0	0.465(9)	0.478(10)	0.499(9)	0.519(8)	0.549(8)
4.8	0.482(9)	0.495(11)	0.516(9)	0.537(9)	0.568(9)
aM_0			$a^{3/2}(f\sqrt{M})^{(1)}$		
2.4	-0.0543(13)	-0.0549(11)	-0.0567(11)	-0.0580(10)	-0.0598(9)
2.9	-0.0480(12)	-0.0486(10)	-0.0500(10)	-0.0513(9)	-0.0530(8)
3.4	-0.0432(11)	-0.0437(9)	-0.0447(8)	-0.0459(9)	-0.0475(8)
4.0	-0.0386(11)	-0.0390(9)	-0.0399(7)	-0.0408(8)	-0.0423(7)
4.8	-0.0339(11)	-0.0342(9)	-0.0350(7)	-0.0356(8)	-0.0370(7)

TABLE XVIII. Decay matrix elements at $\beta=2.334$.

	$K=0.1337$	$K=0.1349$	$K=0.1358$	$K=0.1368$	$K=0.1374$
aM_0			$a^{3/2}(f\sqrt{M})^{(0)}$		
2.4	0.359(8)	0.370(6)	0.389(6)	0.406(5)	0.428(5)
2.9	0.373(8)	0.385(7)	0.405(6)	0.423(5)	0.446(5)
3.4	0.384(9)	0.396(7)	0.418(6)	0.437(6)	0.462(6)
4.0	0.395(10)	0.408(8)	0.430(7)	0.451(6)	0.477(6)
4.8	0.407(11)	0.421(9)	0.444(7)	0.466(7)	0.493(7)
aM_0			$a^{3/2}(f\sqrt{M})^{(1)}$		
2.4	-0.0440(9)	-0.0449(8)	-0.0464(7)	-0.0477(6)	-0.0494(6)
2.9	-0.0389(9)	-0.0396(7)	-0.0410(6)	-0.0423(6)	-0.0438(6)
3.4	-0.0349(8)	-0.0356(7)	-0.0368(6)	-0.0380(6)	-0.0394(5)
4.0	-0.0311(8)	-0.0317(6)	-0.0328(6)	-0.0339(5)	-0.0352(5)
4.8	-0.0272(7)	-0.0277(6)	-0.0287(5)	-0.0296(5)	-0.0309(5)

TABLE XIX. Decay matrix elements at $\beta=2.575$.

	$K=0.1329$	$K=0.1337$	$K=0.1344$	$K=0.1351$	$K=0.1353$
aM_0			$a^{3/2}(f\sqrt{M})^{(0)}$		
2.4	0.221(3)	0.224(3)	0.235(2)	0.247(2)	0.261(2)
2.6	0.224(3)	0.227(3)	0.238(2)	0.251(2)	0.264(2)
2.9	0.228(3)	0.231(3)	0.243(2)	0.255(2)	0.269(2)
3.2	0.231(3)	0.234(3)	0.246(2)	0.259(2)	0.274(2)
3.5	0.234(3)	0.237(3)	0.250(3)	0.263(2)	0.277(2)
aM_0			$a^{3/2}(f\sqrt{M})^{(1)}$		
2.4	-0.0225(4)	-0.0227(3)	-0.0236(3)	-0.0245(3)	-0.0256(2)
2.6	-0.0213(3)	-0.0215(3)	-0.0223(3)	-0.0232(3)	-0.0242(2)
2.9	-0.0197(3)	-0.0199(3)	-0.0207(3)	-0.0215(2)	-0.0225(2)
3.2	-0.0184(3)	-0.0185(3)	-0.0193(2)	-0.0200(2)	-0.0209(2)
3.5	-0.0172(3)	-0.0173(3)	-0.0180(2)	-0.0188(2)	-0.0196(2)

VII. CONCLUSIONS

We have calculated the B meson decay constants in two-flavor full QCD using the $O(1/M)$ NRQCD action, paying attention to the sea quark mass dependence and extrapolation to the chiral limit of the sea quark, as well as to estimates of discretization errors. We have used improved actions for both quarks and gluons to minimize the discretization error at a modest lattice spacing. We also have performed quenched simulations at matching lattice spacings using the same actions, to study the effect of dynamical sea quarks.

We have confirmed a plateau in the plot of the decay constants as a function of lattice spacing for the quenched calculation, but could not see a plateau in the full QCD calculation, within the statistical errors. We have estimated the decay constant in the continuum by evaluating systematic errors from discretization at each lattice spacing.

We have found that the NRQCD action and the relativistic Fermilab formalism give consistent estimates for the B me-

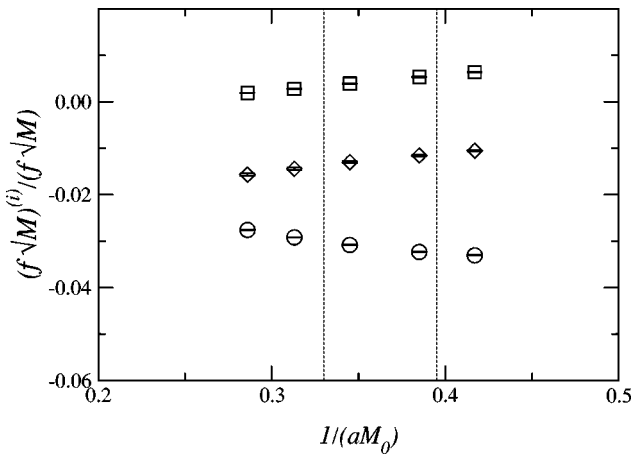


FIG. 8. Relative size of the one-loop corrections to the current matrix elements in full QCD. Circles denote $\alpha_s \rho_0(f\sqrt{M})^{(0)}/(f\sqrt{M})$, squares stand for $\alpha_s \rho_1(f\sqrt{M})^{(1)}/(f\sqrt{M})$, and diamonds give $\alpha_s \rho_2(f\sqrt{M})^{(2)}/(f\sqrt{M})$. The two vertical lines show a band to indicate the position of the bare b quark mass. The parameter values are $\beta=2.1$ and $K_{sea}=K_{val}=0.1382$.

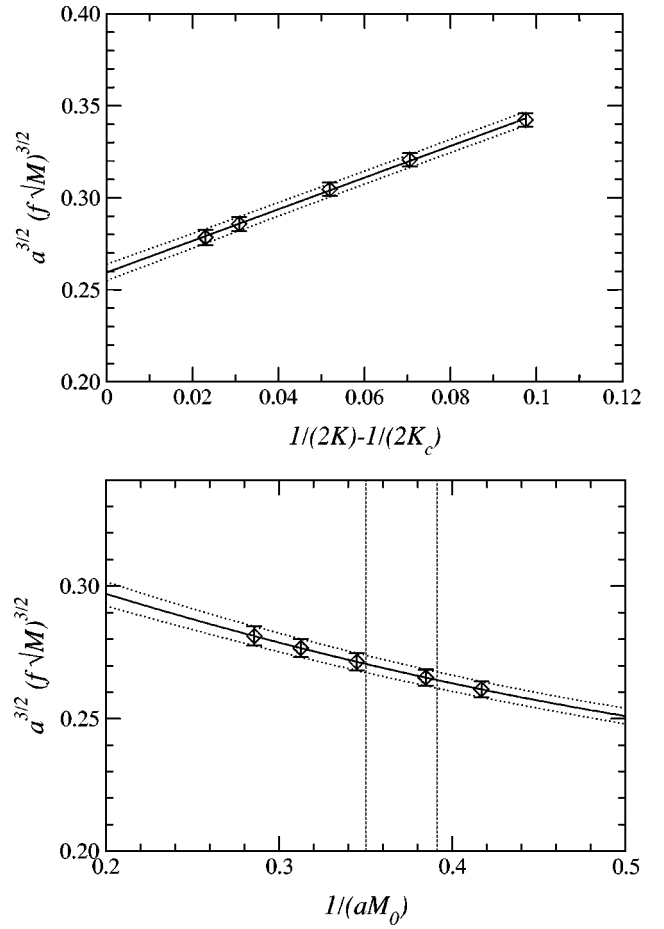


FIG. 9. Decay matrix elements for the parameter values $\beta=2.1$, and $K_{sea}=0.1374$. The top panel shows a fit of $(f\sqrt{M})^{(0)}$ as a function of the light quark mass for $aM_0=2.6$, which is close to M_{0b} . The bottom panel shows a fit of $(f\sqrt{M})$ in the heavy quark mass with the light quark mass interpolated to the strange quark mass. Solid curves denote the fits and dotted lines the error. The vertical lines in the figure on the bottom give the error bounds of aM_{0b} .

TABLE XX. Quenched decay constants.

β	f_B (MeV)	f_{B_s} (MeV)		f_{B_s}/f_B	
		K input	Φ input	K input	Φ input
Scale from m_ρ					
2.187	224(6)	256(5)	265(5)	1.146(10)	1.184(12)
2.281	199(7)	230(6)	239(6)	1.154(20)	1.197(25)
2.334	185(6)	217(5)	226(5)	1.177(18)	1.222(23)
2.575	191(4)	220(4)	226(5)	1.150(9)	1.184(12)
Scale from Y					
2.187	269(8)	295(8)	309(8)	1.094(6)	1.149(9)
2.281	257(9)	282(8)	297(7)	1.096(11)	1.154(18)

TABLE XXI. Partially quenched decay constants.

K_{sea}	f_B (MeV)	f_{B_s} (MeV)		f_{B_s}/f_B	
		K input	Φ input	K input	Φ input
Scale from m_ρ					
		$\beta = 1.95$			
0.1375	230(4)	266(4)	275(4)	1.156(9)	1.194(11)
0.1390	233(7)	266(6)	275(6)	1.144(14)	1.179(17)
0.1400	220(5)	259(4)	268(4)	1.174(10)	1.215(13)
0.1410	228(6)	266(5)	273(6)	1.167(15)	1.200(18)
		$\beta = 2.1$			
0.1357	193(5)	225(5)	232(5)	1.166(12)	1.199(14)
0.1367	206(6)	238(5)	243(6)	1.159(11)	1.184(13)
0.1374	197(5)	231(6)	235(6)	1.172(11)	1.196(12)
0.1382	201(8)	236(9)	242(8)	1.177(15)	1.203(17)
Scale from Y					
		$\beta = 1.95$			
0.1375	264(5)	295(4)	309(4)	1.118(7)	1.168(10)
0.1390	266(10)	294(10)	306(10)	1.108(9)	1.154(13)
0.1400	254(7)	286(6)	300(6)	1.130(7)	1.183(10)
0.1410	259(8)	293(7)	305(7)	1.130(12)	1.176(15)
		$\beta = 2.1$			
0.1357	250(7)	276(7)	289(7)	1.104(9)	1.155(13)
0.1382	249(11)	279(11)	290(11)	1.118(11)	1.162(14)

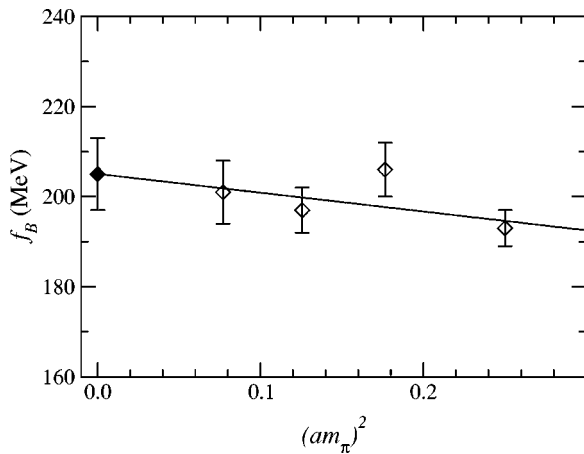
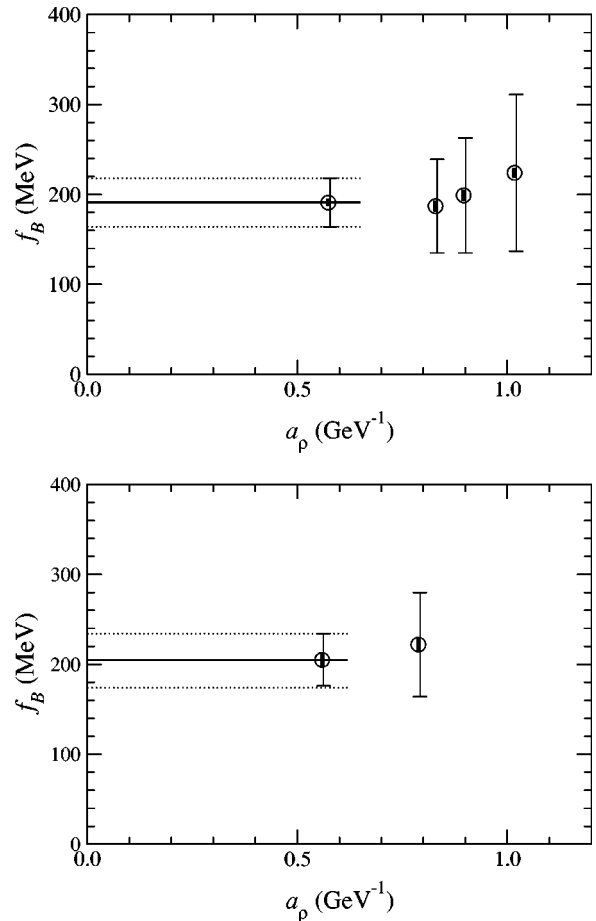
FIG. 10. Decay constant at $\beta=2.1$ as a function of the sea quark mass. Open symbols denote the partially quenched results, the solid line is the fit in $(am_\pi)^2$, and the filled symbol is the value in the chiral limit of the sea quark mass.

TABLE XXII. Decay constants in full QCD.

β	f_B (MeV)	f_{B_s} (MeV)		f_{B_s}/f_B	
		K input	Φ input	K input	Φ input
Scale from m_ρ					
1.95	222(6)	261(5)	268(6)	1.176(14)	1.212(17)
2.1	204(8)	242(9)	245(9)	1.179(18)	1.198(20)
Scale from Y					
1.95	254(8)	287(7)	300(7)	1.134(10)	1.183(14)
2.1	249(16)	280(16)	290(16)	1.124(16)	1.165(21)

son decay constants. Our values of f_B and f_{B_s} are slightly higher than those from previous studies, but the disagreement is at most at 1σ level.

We have confirmed that the sea quark effect makes the decay constants larger by $\approx 10\%$, which is about $(1.5-2)\sigma$ effects in our statistics. The systematic error due to the uncertainty of the strange quark mass (whether it is determined from K or ϕ) is reduced to a negligible level by the intro-

FIG. 11. f_B as a function of the lattice spacing in quenched QCD (top) and full QCD (bottom). Thick error bars denote statistical errors and thin error bars systematic errors. The solid horizontal line shows the final estimate for f_B taken from the finest lattice, and the dashed horizontal lines the error (statistical and systematic added in quadrature) in this estimate.

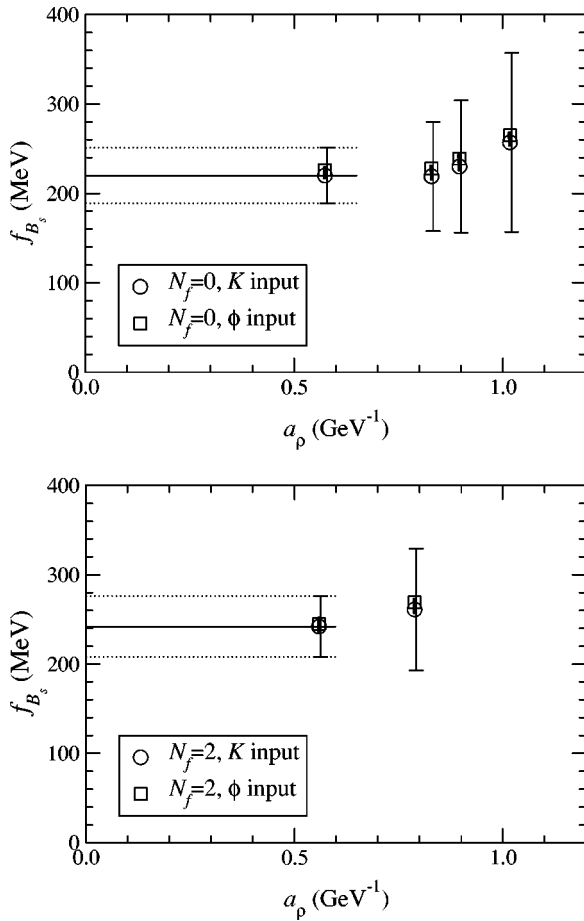


FIG. 12. f_{B_s} as a function of the lattice spacing in quenched QCD (top) and full QCD (bottom). Thick error bars denote statistical errors, and thin ones systematic errors. The solid horizontal line shows the final estimate for f_{B_s} taken from the result on the finest lattice, and the dashed horizontal lines the error in this estimate.

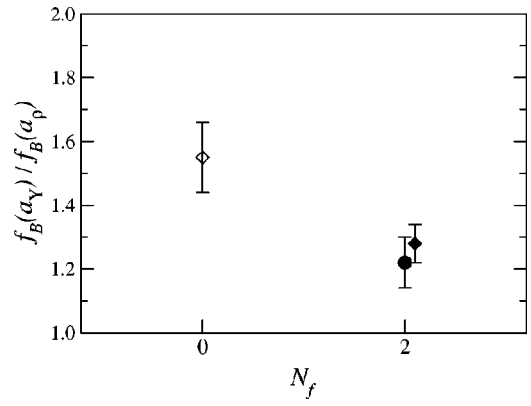


FIG. 13. Ratio of decay constants determined with a_Y and a_ρ for quenched ($N_f=0$) and partially quenched ($N_f=2$) QCD. The filled circle is our results, while the filled diamond is from Ref. [6]. The quenched data (open diamond) have been obtained by reanalyzing the results from Ref. [14] using lattice spacings from the Y.

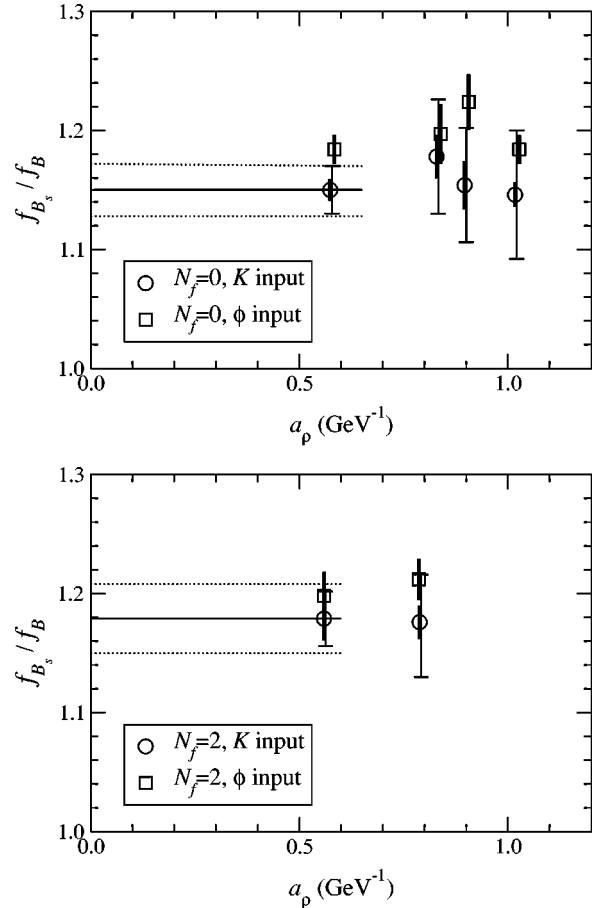


TABLE XXIII. Estimated systematic errors. $\alpha_{\overline{\text{MS}}}(1/a)$ and $\Lambda_{QCD}=600$ MeV are used.

	$N_f=0$ lattices			$N_f=2$ lattices		
β	2.187	2.281	2.334	2.575	1.95	2.1
$O(a^2 \Lambda_{QCD}^2)$	35%	29%	25%	12%	22%	11%
$O(\alpha_s a \Lambda_{QCD})$	13%	11%	10%	6%	11%	7%
$O(\alpha_s^2)$	5%	5%	4%	3%	5%	4%
$O(\alpha_s \Lambda_{QCD} / M_b)$	3%	3%	3%	2%	3%	3%
$O[\alpha_s^2 / (a M_b)]$	1%	1%	1%	1%	1%	2%
$O(\Lambda_{QCD}^2 / M_b^2)$	2%	2%	2%	1%	2%	2%
$O(\Lambda_{QCD}^2 a / M_b)$	8%	7%	7%	4%	6%	4%
Total error for f_B and f_{B_s}	39%	32%	28%	14%	26%	14%
Total error for $f_{B_s}/f_B - 1$	37%	31%	27%	13%	25%	13%

FIG. 14. f_{B_s}/f_B as a function of the lattice spacing in quenched QCD (top) and full QCD (bottom). Thick error bars denote statistical errors, and thin ones systematic errors. The solid horizontal line shows the final estimate for f_{B_s}/f_B taken from the finest lattice, and the dashed horizontal lines the error in this estimate.

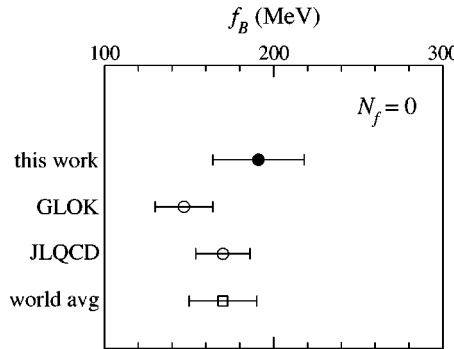


FIG. 15. Comparison of quenched results for f_B from NRQCD. The filled circle denotes the quenched result quoted in this paper, while the two open circles show results from other recent NRQCD studies [14,15]. The open square stands for the quenched world average quoted in Ref. [1]. Errors include statistical and systematic errors combined in quadrature.

duction of two flavors of dynamical sea quarks. Comparing the results using the lattice scales from the ρ meson mass and the Υ mass splitting, we find that the uncertainty from the lattice scale is also smaller in full QCD, but remains to give a substantial error to the decay constants.

Our final result for the decay constant is summarized as

$$f_B^{N_f=2} = 204 \pm 8 \pm 29^{+44}_{-0} \text{ MeV}, \quad (33)$$

$$f_{B_s}^{N_f=2} = 242 \pm 9 \pm 34^{+38}_{-0} \text{ MeV}, \quad (34)$$

$$\frac{f_{B_s}^{N_f=2}}{f_B^{N_f=2}} = 1.179 \pm 18 \pm 23, \quad (35)$$

where the central values are taken from those using the lattice scale from the ρ meson mass, because the B physics will

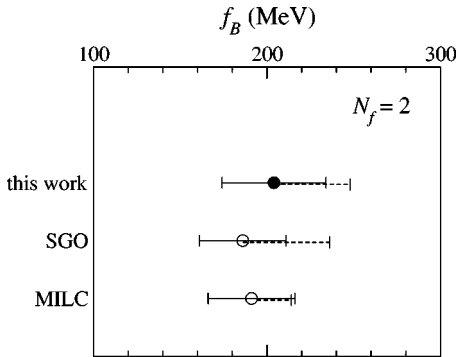


FIG. 16. Comparison of results for f_B in $N_f=2$ QCD. The filled circle denotes the result quoted in this paper for $N_f=2$, and the two open circles stand for the results from Refs. [6] and [7]. Solid error bars include statistical and systematic errors combined in quadrature. The uncertainty from setting the lattice spacing from light physics quantities or Υ spectroscopy is shown separately by dotted lines.

be governed by the soft hadron phenomena, and the uncertainty from the lattice scale is shown by the third error. This uncertainty cancels out in the ratio f_{B_s}/f_B . We should take these values as provisional until a plateau is actually confirmed with a future dynamical calculation.

ACKNOWLEDGMENTS

The calculations were performed on the parallel computer CP-PACS at the Center for Computational Physics, University of Tsukuba. This work was supported in part by Grants-in-Aid from the Ministry of Education (Nos. 09304029, 10640246, 10640248, 10740107, 11640250, 11640294, and 11740162). T.M. and A.A.K. was supported by the JSPS Research for the Future Program (Project No. JSPS-RFTF 97P01102). S.E., K.N., and H.P.S. are JSPS Research Fellows.

-
- [1] S. Hashimoto, in Proceedings of the International Symposium on Lattice Field Theory, Pisa, Italy, 1999 [Nucl. Phys. B (Proc. Suppl.) **83-84**, 3 (2000)].
- [2] C. Bernard, in Proceedings of the International Symposium on Lattice Field Theory, Bangalore, India, 2000 [Nucl. Phys. B (Proc. Suppl.) **94**, 159 (2001)].
- [3] A.X. El-Khadra, A.S. Kronfeld, and P.B. Mackenzie, Phys. Rev. D **55**, 3933 (1997).
- [4] B.A. Thacker and G.P. Lepage, Phys. Rev. D **43**, 196 (1991); G.P. Lepage *et al.*, *ibid.* **46**, 4052 (1992).
- [5] CP-PACS Collaboration, A. Ali Khan *et al.*, Phys. Rev. D (to be published), hep-lat/0010009.
- [6] S. Collins, C.T.H. Davies, U.M. Heller, A. Ali Khan, J. Shigemitsu, J. Sloan, and C. Morningstar, Phys. Rev. D **60**, 074504 (1999).
- [7] MILC Collaboration, C. Bernard *et al.*, Phys. Rev. Lett. **81**, 4812 (1998); in Proceedings of the International Symposium on Lattice Field Theory, Pisa, Italy, 1999 [Nucl. Phys. B (Proc. Suppl.) **83-84**, 289 (2000)]; in Proceedings of the International Symposium on Lattice Field Theory, Bangalore, India, 2000 [*ibid.* **94**, 346 (2001)].
- [8] Y. Iwasaki, Nucl. Phys. **B258**, 141 (1985); University of Tsukuba Report No. UTHEP-118, 1983.
- [9] B. Sheikholeslami and R. Wohlert, Nucl. Phys. **B259**, 572 (1985).
- [10] R. Burkhalter, in Proceedings of the International Symposium on Lattice Field Theory, Boulder, USA, 1998 [Nucl. Phys. B (Proc. Suppl.) **73**, 3 (1999)].
- [11] CP-PACS Collaboration, A. Ali Khan *et al.*, Phys. Rev. Lett. **85**, 4674 (2000).
- [12] CP-PACS Collaboration, A. Ali Khan *et al.*, hep-lat/0105015.
- [13] K.-I. Ishikawa, H. Matsufuru, T. Onogi, N. Yamada, and S. Hashimoto, Phys. Rev. D **56**, 7028 (1997).
- [14] A. Ali Khan, S. Collins, C.T.H. Davies, C. Morningstar, J. Shigemitsu, and J. Sloan, Phys. Lett. B **427**, 132 (1998).
- [15] JLQCD Collaboration, K.-I. Ishikawa *et al.*, Phys. Rev. D **61**, 074501 (2000).
- [16] C.T.H. Davies, K. Hornbostel, A. Langnau, G.P. Lepage, A.

- Lidsey, J. Shigemitsu, and J. Sloan, Phys. Rev. D **50**, 6963 (1994).
- [17] K.-I. Ishikawa, T. Onogi, and N. Yamada, in Proceedings of the International Symposium on Lattice Field Theory, Pisa, Italy, 1999 [Nucl. Phys. B (Proc. Suppl.) **83-84**, 301 (2000)].
- [18] C.J. Morningstar and J. Shigemitsu, Phys. Rev. D **57**, 6741 (1998).
- [19] CP-PACS Collaboration, T. Manke *et al.*, Phys. Rev. D **62**, 114508 (2000).
- [20] A. Ali Khan, T. Bhattacharya, S. Collins, C.T.H. Davies, R. Gupta, C. Morningstar, J. Shigemitsu, and J. Sloan, Phys. Rev. D **62**, 054505 (2000).
- [21] J. Hein, S. Collins, C.T.H. Davies, A. Ali Khan, H. Newton, C. Morningstar, J. Shigemitsu, and J. Sloan, Phys. Rev. D **62**, 074503 (2000).
- [22] G.P. Lepage and P. Mackenzie, Phys. Rev. D **48**, 2250 (1993).
- [23] C.T.H. Davies, K. Hornbostel, G.P. Lepage, A. Lidsey, P. McCallum, J. Shigemitsu, and J. Sloan, Phys. Rev. D **58**, 054505 (1998).
- [24] S. Collins, C.T.H. Davies, J. Hein, G.P. Lepage, C.J. Morningstar, J. Shigemitsu, and J. Sloan, Phys. Rev. D **63**, 034505 (2001).